NATIONAL ADVISORY COMMITTEE FOR AERONAUTICS

TECHNICAL NOTE 3656

A SELF-BALANCING LINE-REVERSAL PYROMETER

By Donald Buchele

Lewis Flight Propulsion Laboratory
Cleveland, Ohio

Washington
August 1956

TABLE OF CONTENTS

the mechanical design of the instrument or in the method of analysis, that prevents substitution of some other suitable spectral line in the visible region.

This work is part of the research program in high-temperature measurements currently conducted at the NACA Lewis laboratory.

PRINCIPLE OF INSTRUMENT

When certain compounds are added to a hot gas, their atoms radiate monochromatic light. A spectral line may then be observed through a spectroscope. Also, the radiation from a lamp shining through the gas to a spectroscope may be observed as a continuous spectrum extending from the line. The spectral line appears brighter than the continuum if the lamp temperature is low enough. As the lamp temperature is increased, the continuum brightness becomes equal to and then greater than the brightness of the spectral line. When the spectral-line brightness matches the continuum, the line disappears and the state of line reversal exists. Line reversal is based on Kirchhoff's law, which states that emissivity equals absorptivity at any wavelength.

At line reversal the lamp temperature is uniquely related to the gas temperature when thermal equilibrium exists between the gas and the atoms of the added compound. A lamp calibration then gives the gas temperature in terms of lamp current.

The pyrometer described in this paper replaces the two conventional manual operations of the line-reversal method, namely, observing the spectral line through a spectroscope and controlling the lamp current to produce reversal. The self-balancing pyrometer, shown in figure 1, consists of an enclosed optical unit that projects a light beam across the gas to a reflector. The light is reflected back to the optical unit, which contains a spectroscope and a photocell that detects deviations from reversal of the spectral line. The photocell signal is sent to an electrical unit containing a self-balancing system which adjusts the current through the lamp in the optical unit to restore the state of reversal. The lamp current, related to the gas temperature by a previous calibration, is continuously indicated by the ammeter.

Principal details of the self-balancing system are shown in figure 2. The spectroscope prism receives light from both the colored gas and the lamp through aperture S_1 and entrance slit S_2, and the spectrum is focused at the plane of the exit slit S_3. Slit S_3 vibrates sinusoidally at 60-cps line frequency and is positioned along the spectrum to transmit light to the photomultiplier from the spectral line at the slit center position, from a shorter adjacent wavelength in the continuum at

one peak of amplitude, and from a longer adjacent wavelength in the continuum at the other peak of amplitude. As the slit vibrates, flux from the spectral line is compared alternately with flux from the two adjacent wavelengths during each cycle of slit motion. When the spectral line is not at reversal, a difference of light flux between the spectral line and the adjacent wavelengths generates a 120-cps signal. The signal is transmitted from the photomultiplier to the self-balancing amplifier, motor, and variable transformer, which then adjusts the lamp current to restore the state of line reversal.

ANALYSIS

The radiation terminology to be used follows the definitions of reference 3.

Under blackbody conditions, the monochromatic areal intensity of a radiating source is given by Planck's equation (symbols defined in appendix A):

$$N_{\lambda,b} = c_1 \lambda^{-5} \left(e^{\frac{c_2}{\lambda T_b}} - 1 \right)^{-1} \tag{1}$$

For nonblackbody conditions, including an optical transmission factor τ between the radiating source and the point of observation, the monochromatic areal intensity at the point of observation is

$$N_\lambda = \tau_\lambda \varepsilon_\lambda N_{\lambda,b} \tag{2}$$

The monochromatic areal intensity is defined in terms of radiant flux as

$$N_\lambda = \frac{d^3\varphi}{dA\, d\omega\, d\lambda} \tag{3}$$

or

$$\varphi = A\, \omega \int_{\lambda_1}^{\lambda_2} \tau_\lambda \varepsilon_\lambda N_{\lambda,b}\, d\lambda \tag{4}$$

This analysis will be concerned with reversal of the sodium D-lines. In figure 3 the monochromatic areal intensity N_λ at the spectroscope is shown plotted as a function of wavelength with the two D-lines shown bright, dark, and at reversal. Let the spectral-line width of one D-line at its half-maximum areal intensity be $\Delta\lambda_t$. (The width at the half-maximum will be termed the "band width.") The band width $\Delta\lambda_d$ transmitted by the spectroscope slit may have to be made considerable greater than

$\Delta\lambda_t$ because of limited resolution of the spectroscope, or it may be so chosen in order to gain the increased light flux. Furthermore, the width $\Delta\lambda_t$ may change by a factor as large as 20 as the concentration of the sodium atoms in the flame changes. In this instrument $\Delta\lambda_d$ of 12 A was chosen to be large enough to span both D-lines, which have 6-A separation.

Also indicated in figure 3 are the wavelength intervals transmitted by slit S_3 during 1 cycle of its sinusoidal motion. The two peaks of slit amplitude correspond to center wavelengths of $\lambda_c = 5881$ A and $\lambda_e = 5905$ A, and to respective band widths of $\lambda_2 - \lambda_1 = \Delta\lambda_c$ and $\lambda_4 - \lambda_3 = \Delta\lambda_e$. The center position of motion corresponds to a center wavelength $\lambda_d = 5893$ A having a band width $\Delta\lambda_d = \lambda_3 - \lambda_2 \approx 12$ A which contains both D-lines.

In figure 4 are shown the light fluxes transmitted by the slit to the photocell, during 1 cycle of slit motion, when the D-lines are brighter, equal to, or darker than the adjacent spectrum. The alternating component of light flux is zero at reversal. The alternating component has a 180° phase shift as reversal is passed through, from a bright D-line to a dark D-line. A phase-sensitive self-balancing system can detect the state of reversal.

Slit S_3 oscillates between two predetermined wavelengths. This may cause an error in reversal determination because both the photocell sensitivity and the lamp intensity vary with wavelength. Other errors may arise because of reflection from the lamp filament, variation of sodium content of the gas, and dirtying of the windows. Some of these errors shift the temperature indication; others reduce the sensibility of measurement. The following development of the reversal equations will include these effects, establish the magnitude of the errors they introduce, and show how these errors are reduced or avoided by appropriate instrument design.

Single-Pass System

For convenience in derivation of instrument errors, the conventional single-pass optical system will be considered first. Then, assuming that some instrument errors are eliminated by an appropriate design, the addition of a reflector for the double-pass system will be considered.

The components of the light flux shown in figure 5 are used to write the reversal equation, equation (B9), in appendix B. One flux component includes the lamp reflection factor ρ_l, because the ribbon-filament surface is assumed to be perpendicular to the optical axis. The reflection

factor may be considered zero if the filament is tilted enough to reflect light away from the condensing-lens aperture. In this instrument the condensing-lens aperture ratio is too large to permit sufficient tilt.

Manipulation of the reversal equation yields a photocell signal current that has both 60- and 120-cps components. The 60-cps current can be almost eliminated by a suitable color filter τ_4 as specified in appendix B, equation (B7). The self-balancing system operates to reduce the 120-cps current to zero. At this balance point, the reversal equation (eq. (B9), appendix B) can be written as

$$N_{d,g} = \tau_1 \varepsilon_{d,l} N_{d,l} - \tau_1^2 \rho_2 (1 - \varepsilon_r) N_{d,g} + \Delta N_{d,l} \tag{5}$$

where $\Delta N_{d,l}$ is defined in equation (B9), and an effective emissivity ε_r is defined as

$$\varepsilon_r \equiv \frac{\int_{\lambda_2}^{\lambda_3} \varepsilon_{d,g}^2 \, d\lambda}{\int_{\lambda_2}^{\lambda_3} \varepsilon_{d,g} \, d\lambda} \tag{6 or B10}$$

The condition in equation (5) when the last two terms on the right side of the equation are zero represents the idealized condition; that is, the monochromatic areal intensity $N_{d,g}$ that the gas would possess if it were a blackbody is equal to the monochromatic areal intensity $\tau_1 \varepsilon_{d,l} N_{d,l}$ of the lamp radiation at the gas location. The lamp radiation is assumed to have been correlated with the temperature of a blackbody at the gas location by calibration with an optical pyrometer.

The second term on the right side of equation (5) exists when either the gas or the lamp is not a blackbody. The first two terms are a single-pass-system calibration equation:

$$N_{d,g} = \tau_1 \varepsilon_{d,l} N_{d,l} \tau_1' \tag{7}$$

where

$$\tau_1' = \frac{1}{1 + \tau_1^2 \rho_l (1 - \varepsilon_r)} \tag{8}$$

Table I lists the values of τ_1' for representative values of τ_1, with $\rho_l = 1 - \varepsilon_l = 0.57$, calculated from equation (8). If the value of ε_r is not known, a value of τ_1' corresponding to a median value $\varepsilon_r = 0.5$ may be assumed. The limit of temperature error made by this assumption ranges from ±1.6 percent for $\tau_1 = 0.85$ to ±0.2 percent for $\tau_1 = 0.3$. The effective emissivity ε_r may be measured by the procedure described in appendix B.

The third term on the right side of equation (5) represents an error. This error would be zero only if the photocell sensitivity μ, the filter transmissivity τ_4, the lamp emissivity ε_l, the lamp monochromatic areal intensity N_l, and the dispersion of the glass of the spectroscope prism all varied linearly with wavelength λ in the region $\lambda_c \leq \lambda \leq \lambda_e$. Since at least some of the preceding quantities vary nonlinearly with wavelength, an error results that causes a shift of temperature indication. The error is considered as an apparent change $\Delta N_{d,l}$ in the value of $N_{d,l}$. This apparent change in lamp radiation may be related to the change in temperature indication by differentiating Planck's radiation equation. This equation yields the error in temperature indication caused by the nonlinearities:

$$\Delta T_l = \frac{\lambda_d T_l^2}{c_2} \frac{\Delta N_{d,l}}{N_{d,l}} \tag{9}$$

The error ΔT_l varies inversely as $\int_{\lambda_2}^{\lambda_3} \varepsilon_{d,g} d\lambda$ (eq. (B9)), which depends on the concentration of sodium atoms. The error contributed by nonlinearities is minimized by injecting an appropriately phased 120-cps electric bucking signal into the photocell voltage supply. In the present instrument, the original error $\Delta T_l / T_l$ was as much as 2 percent near to the low-temperature limit of the instrument; this error is reduced by the bucking signal by a factor of at least 3.

Double-Pass System

In the analysis without reflector, three center wavelengths λ_c, λ_d, and λ_e were used to derive and to point out the errors of the self-balancing system. These errors have been substantially eliminated (by use of an appropriate color filter and an appropriately phased electric

bucking voltage); so it is now possible to study the effect of the reflector alone. The components of the light flux shown in figure 6 are used to write the reversal equation, equation (B18), in appendix B. Manipulation of the equation yields the calibration equation for a double-pass system:

$$N_{d,g} = \tau_1 \epsilon_{d,l} N_{d,l} \tau_3' \qquad (10) \text{ or } (B20)$$

where

$$\tau_3' = \tau_3(1 + \rho_l \tau_1^2 \tau_3) \frac{2 - \epsilon_r}{1 + \tau_3(1 - \epsilon_r)} \qquad (11) \text{ or } (B21)$$

Equation (11) represents solely the effect of a reflector and the doubled-light-path length through the gas, including lamp-filament reflection.

Table II lists the values of τ_3' for representative values of τ_1 and τ_3, with $\rho_l = 1 - \epsilon_l = 0.57$, calculated from equation (11). If the value of ϵ_r is not known, a value of τ_3' corresponding to a median value $\epsilon_r = 0.5$ may be assumed. The limit of temperature error made by this assumption ranges from ±0.4 percent for $\tau_1 = 0.3$ and $\tau_3 = 0.7$ to ±0.2 percent for $\tau_1 = 0.4$ and $\tau_3 = 0.9$.

DESIGN

Optical Unit

Construction of the optical unit is shown by the photographs of figure 7. All the components are attached to a 1/4-inch-thick Duraluminum plate which is suspended inside a sheet-metal case by three vibration-insulating mounts. The light projection components (fig. 7(a)) are all located on one side of the plate. The spectroscope and photocell components (fig. 7(b)) are attached to the other side of the plate. The weight of the assembly in its case is 26 pounds.

Both the optical unit and prism reflector are demountable from mounting plates to which they are secured by two thumb screws. The mounting plates may be permanently attached to the test apparatus or other structure. The projection lamp must be operated base down for proper cooling.

The final alinement of the optical unit with the prism reflector can be performed from the outside of the case by means of an auxiliary, built-in lamp and mirror system. The reflector face can be viewed through an

opening in the optical-unit case, and the optical assembly can be moved inside the case until the projected image of the lamp filament is centered on the reflector face. An eyepiece is provided to permit visual observation of the spectrum to check the reversal point.

All essential components of the optical system are shown in figure 8. Their specifications are listed in table III. Photometric design considerations are outlined in reference 4.

Reflector

The light beam leaving the optical unit is almost parallel, the spectroscope requires only a central core of the projected light, and the reflector is of the corner-cube type. As a result of these features, the reflector, after initial alinement, may be rotated and translated an appreciable amount in any direction without introducing sufficient optical misalinement to cause measurement error. The benefits of this tolerance are

(1) The optical unit and reflector may be mounted independently, a rigid connecting structure being unnecessary.

(2) The assembly of components in the optical unit may be suspended by rubber vibration isolators within the protective case.

(3) No error is caused by refraction of the light beam in gas temperature gradients. The refraction would otherwise deflect the light beam partly off the optical-unit objective lens.

An unobstructed distance up to 5 feet separating the reflector and optical unit was chosen as a practical maximum. When the gas temperature is surveyed along the light beam, the space volume observed at any instant has a cross section 0.2 inch high by 0.7 inch wide and a depth occupied by the sodium vapor.

Compensation for Ambient Temperature and Pressure

The spectroscope design, shown in figure 8, avoids appreciable drift of the D-line from slit S_3 due to thermal expansion or to acceleration. However, drift is caused by a change of angular deviation of light through the prism. Angular deviation is affected by a glass refractive-index change with temperature and an air refractive-index change with temperature and barometric pressure. If, initially at temperature T_1, wavelength λ_d, and refractive index n, the prism and air temperatures are changed to T_2, a new wavelength is transmitted to slit S_3, since the slit position corresponds to a particular value of n.

The expressions for wavelength shift due to temperature and pressure are

$$\left(\frac{d\lambda}{dT}\right)_n = -\left(\frac{\partial\lambda}{\partial n}\right)_{gl} \frac{\partial n}{\partial T} \tag{12}$$

$$\left(\frac{d\lambda}{dp}\right)_n = -\left(\frac{\partial\lambda}{\partial n}\right)_{gl} \frac{\partial n}{\partial p} \tag{13}$$

For representative values,

$$\left(\frac{\partial n}{\partial\lambda}\right)_{gl} = -1.5\times10^{-5}\ A^{-1}$$

$$\left(\frac{\partial n}{\partial T}\right)_{gl} = 3.5\times10^{-6}/^{o}R \quad \text{at } 528^{o}\ R$$

$$\left(\frac{\partial n}{\partial T}\right)_{a} = -0.55\times10^{-6}/^{o}R \quad \text{at } 528^{o}\ R$$

$$\left(\frac{\partial n}{\partial p}\right)_{a} = 2.9\times10^{-4}\ atm^{-1}$$

The resulting effects are

$$\left(\frac{d\lambda}{dT}\right)_n = 0.27\ A/^{o}R$$

$$\left(\frac{d\lambda}{dp}\right)_n = 19\ A/atm$$

These values show that usual ambient-temperature changes produce a greater wavelength shift than usual barometric changes. Therefore, temperature compensation in the instrument is effected by using a pair of bimetal strips to translate the spectroscope lens normal to the optical axis; barometric-pressure compensation is omitted.

Effect of Tunnel Windows

If the gas is enclosed, windows must be provided in the enclosure walls. The windows then become part of the optical system.

In the calibration, there is only a single pass of light through the tunnel windows. However, during normal use of the instrument, there is a

double pass of light through the windows, and the reflector is used. If the window and reflector surfaces possess nonzero reflectance, and if the window surfaces are positioned normal to the light path, the several reflections of light from the glass surfaces will affect the reversal indication. Errors of -20° to -30° R can be obtained. These errors can be reduced by coating all surfaces for minimum reflectance at about 6200 A; the errors can be avoided by tilting the windows about 5°. The reflector surface and the elements of the optical unit are already coated for low reflectance or are tilted.

Since the window transmission factor is included in the calibration, the calibration will be changed if the windows become dirty. To keep the windows clean, the windows may be set back from the gas stream by a length of metal pipe and shielded by injecting a constant flow of clean air which flows from the window toward the gas. The windows should preferably also be shielded by a shutter which opens only when a reading is taken.

Electrical Circuit of System

A simplified circuit of the system is shown in figure 9. A constant-voltage transformer regulates the line voltage to a high-voltage direct-current power supply for the photomultiplier and also to two cascaded variable autotransformers which control the voltage applied to a 12.6-volt-lamp transformer.

The lamp-transformer output is rectified full wave and filtered by bridged-T null networks which are tuned to the 120-cycle and 240-cycle ripple frequencies. The ribbon-filament lamp also acts as a long-time-constant filter for thermal fluctuation; so the light output is steady.

Light from the lamp, after passing through the optical system, is converted to a current by the photomultiplier. To correct for the nonlinearities treated in the ANALYSIS section, a 120-cycle component is added to the photomultiplier dynode voltage by a full-wave rectifier circuit. The alternating component of the photocurrent flows through a 120-cycle tuned transformer to the amplifier, where it is converted to 60 cycles and amplified as required to drive the self-balancing motor. This frequency conversion circuit, shown in figure 10, prevents motor drive by an out-of-phase 120-cycle input or any phase 60-cycle input. In the circuit following the frequency converter is a band-pass filter, tuned to 60 cycles, which attenuates the unwanted harmonics. A flat-top transfer characteristic of 30-cycle band width is obtained by feedback through a null circuit consisting of cascaded parallel-T and bridged-T networks.

Stability of Self-Balancing System

A prototype self-balancing system, including the ribbon-filament lamp and photomultiplier in a self-balancing loop, was used to test the stability characteristics of the system. It was found that satisfactory performance could be obtained at all temperature indications if

(1) The radiant flux sensibility of the self-balancing system was proportional to the flux on the photomultiplier.

(2) The self-balancing system changed the lamp voltage at a rate that was proportional to the lamp voltage. This change of lamp voltage is produced in the instrument by cascading a two-gang variable-voltage autotransformer, as shown in figure 9.

The lamp brightness increases approximately as the 12^{th} power of temperature at the D-line wavelength. As specified by condition (1), the corresponding radiant flux must be matched by increased sensibility. The sensibility increase is obtained by reducing the photomultiplier dynode voltage as the temperature rises. This is done by ganging the high-voltage potentiometer in figure 9 to the motor and variable-voltage transformers and shunting the potentiometer at two taps on the winding.

Photomultiplier Noise

Associated with the photomultiplier cathode direct currents i_{dc} due to light flux and thermionic current i_t is an alternating noise current i_n (ref. 5):

$$i_n = \sqrt{2e\,\Delta f(i_t + i_{dc})}$$

where e is the charge on an electron, 1.6×10^{-19} coulomb. The maximum value of the 120-cycle signal current i_s at deviation from line reversal is, in this instrument using both D-lines,

$$i_s = i_{dc}\frac{2\Delta\lambda_t}{\Delta\lambda_d} \approx \frac{i_{dc}}{6}$$

The signal-to-noise ratio is

$$\frac{i_s}{i_n} = \frac{1}{6}\sqrt{\frac{i_{dc}}{2e\,\Delta f}}$$

where $i_t << i_{dc}$. The light flux transmitted by the spectroscope is so small that the root-mean-square noise current is on the order of the

sensibility at low-temperature indications. Therefore, the noise must be reduced by limiting the frequency response Δf by means of a filter. Three filters are used. Two of them are within the self-balancing loop even though the stability of the self-balancing system is thereby reduced. One filter within the loop is the photomultiplier output transformer, resonated at 120 cycles by a condenser. The second filter is the one within the amplifier. Outside the loop, a filter is provided for the lamp ammeter input. This filter has a high-frequency cut-off point considerably lower than that of the filters within the loop.

The cascaded variable-voltage transformer is advantageous at low temperatures, where it decreases the rate of lamp temperature change with self-balancing motor rotation.

Sodium-Compound Injector

Injection of a salt-water solution or spray into the gas stream was found to be troublesome because of clogging of the metering devices by caked salt. However, injection of a dry dust of sodium bicarbonate was satisfactory. Powder is metered by the device shown in figure 11. A motor-driven circular saw blade is immersed in the powder. As the blade rotates, each tooth space carries a few grains into a slot where air flowing through a drilled passage swept by the tooth spaces serves to carry away the grains to the injector probe. An air flow rate of 2 cubic feet per hour is sufficient. When the saw speed is varied over a 600:1 ratio, the rate of powder flow follows in proportion. A range from 3.7×10^{-7} to 2.2×10^{-4} pounds per second is provided. Powder flows only when the saw rotates. However, the air flow is maintained at all times during operation to prevent possible clogging at the probe tube end by condensed moisture.

The 1-inch-diameter saw blade is driven by a 1/75-horsepower, synchronous motor through its 1:6 speed reducer and a pair of tandem-connected speed changers of continuously variable ratio, each speed changer having a ratio range of 1/35 to 5/7.

OPERATION

Alinement of Ribbon-Filament Lamp with Spectroscope

Precise alinement of the ribbon-filament lamp is obtained by use of the alinement lamp built into the optical unit of figure 2. A small mirror is introduced between S_2 and the spectroscope prism, and the alinement-lamp filament is focused on S_2, which then acts as a source of light. The beam is projected from S_2 to the splitter plate and out from

the optical unit, where it defines the external optical axis of the instrument. A screen placed at the reflector shows the physical location of the optical axis. Now the ribbon-filament lamp is turned on, and its filament image is focused on the screen. The ribbon-filament lamp is then moved as required to center its projected light beam about the other one previously observed on the screen. The optical axes are now coaxial.

Alinement of Optical Unit with Reflector

The optical unit is alined with the reflector by using the alinement lamp. The projected beam should be centered on the apex of the reflector. The position of the beam may be observed on a target placed over the central area of the reflector face. When the installation of the reflector and optical unit prevents a direct view of the target, a built-in mirror system temporarily inserted between the splitter plate and the condensing lens reflects the line of sight to the back of the optical unit from where the target can be observed.

Calibration

For calibration, a conventional monochromatic optical pyrometer of the disappearing-filament type replaces the reflector and its adjacent window. The pyrometer is focused on the lamp filament, and the relation between the lamp-current and the optical-pyrometer reading is determined. (Details of the calibration technique are presented in appendix C.) The optical-pyrometer reading gives the "brightness of the lamp at the gas location." The lamp current can be varied manually by turning the variable transformer (fig. 2) by means of the knob on the side of the electrical unit (fig. 1). A tabulation of lamp current against pyrometer indication is obtained.

A temperature correction to the optical-pyrometer readings is then made for the lamp-filament emissivities at the pyrometer wavelength of 6650 A and the D-line wavelength of 5893 A, and also for the transmission factor τ_1. The correction is derived in appendix C. Further correction is then made for the factor τ_3'. These corrections are made by use of figures 12 and 13 and table II.

Table IV shows the steps in the lamp calibration involving, successively, the observation of the optical-pyrometer reading, correction for typical values of ε_l and τ_1, and correction for τ_3'. A calibration curve is prepared from the initial and final columns.

Sodium Injection Rate

The quantity $\int_{\lambda_2}^{\lambda_3} \varepsilon_{d,g} d\lambda$ strongly affects reversal sensitivity. This is shown by equation (B9), appendix B, where the sensitivity to the difference of monochromatic areal intensity $\tau_1 \varepsilon_{d,l} N_{d,l} - N_{d,g}$ is proportional to the product $C\mu_d \tau_2 \tau_{d,4} \int_{\lambda_2}^{\lambda_3} \varepsilon_{d,g} d\lambda$. Also, by equation (B9), the correction for the nonlinearities varies inversely with $\int_{\lambda_2}^{\lambda_3} \varepsilon_{d,g} d\lambda$. It is therefore desirable that the integral be large. This is obtained when the amount of sodium injected is large, as illustrated in figure 14 for the spectral absorption of one D-line. The area between any curve and the line $N_\lambda = N_0$ is proportional to $\int_{\lambda_2}^{\lambda_3} \varepsilon_{d,g} d\lambda$. This area is a measure of the signal power available to a detector of reversal.

The curve for $k_0 y << 1$ is obtained when a very small amount of sodium is in the gas, so that the absorptivity $\alpha_{d,g}$ is less than 1, and the half-maximum band width $\Delta\lambda_t$ is about 0.1 A at atmospheric pressure. As the amount of sodium is increased, $k_0 y > 1.0$, the absorptivity at λ_0 is close to a maximum of 1.0; and then, as the amount increases further, $k_0 y >> 1$, the band width $\Delta\lambda_t$ increases to as much as several angstroms.

Optimum sensibility for visual observation of one D-line is obtained when $\alpha_{d,g} = 1.0$ at λ_0, and $\Delta\lambda_t$ is at least as great as the resolution $\Delta\lambda_d$ of the spectroscope. For the instrument itself, sufficient line absorption is obtained when $\alpha_{\lambda,g} = 0.5$ at wavelengths 0.5 A from each side of the center wavelength λ_0 of one D-line. This criterion has been chosen for the rate of sodium injection derived in appendix D.

If a vaporizing efficiency of 100 percent is assumed, the rate w of sodium bicarbonate injection as derived in appendix D, equation (D10), is

$$\left.\begin{aligned} w &\approx C_1 \frac{My}{p} \qquad p < 20 \text{ atm} \\ w &\approx C_2 Myp \qquad p > 20 \text{ atm} \end{aligned}\right\} \tag{14}$$

where

$C_1 = 5.9 \times 10^{-6}$ lb atm in.$^{-1}$ sec^{-1}

$C_2 = 1.38 \times 10^{-8}$ lb atm^{-1} in.$^{-1}$ sec^{-1}

The injection rate w is expressed in terms of readily measurable gas stream quantities (Mach number M, static pressure p, and path length y) through a cylindrically shaped stream of sodium vapor.

5797

An upper limit of the gas pressure p is set by the half-maximum D-line width $\Delta\lambda_t$, which increases with pressure. A width of 3 A is the maximum that should be used with the existing amplitude of motion of slit S_3 in the instrument. The upper limit of the gas pressure corresponding to 3 A is given approximately by equation (D4), appendix D, and is 61 atmospheres. This limit can be extended if the amplitude of slit motion is increased.

The gas tends to be cooled by the added mass of both the sodium compound and the air that transports it through the injector probe. The cooling due to air can be estimated from its flow rate of approximately 2 cubic feet per hour. The cooling effect is usually negligible at 1 atmosphere of pressure.

Gas Contamination

In practice, the cross section of the gas may be contaminated with sodium, small luminous particles such as carbon, or larger particles of foreign material. This contamination can introduce a temperature error if the gas temperature is not constant along the light path or if the particles are not at the gas temperature.

If sodium contamination is significant, the instrument will indicate an "average" gas temperature before the local sodium injection. After local injection a different temperature may be indicated, but this temperature is incorrect by an amount dependent upon the relative optical strengths of the contamination and local injection. Correction for the error is not considered herein. It is complicated because the emissivity of contaminating sodium is a rapidly varying function of wavelength. Instead of a correction, the contamination should be avoided. If that is not possible, an element such as lithium, which is not likely to contaminate the gas, could be used.

The error due to contamination by particles such as carbon or foreign material can be estimated or corrected by a method derived in appendix E for a single- as well as a double-pass system. The method is valid for

a contaminant emissivity in the range between 0 and 0.1, a particle temperature different from the gas temperature, and takes into account the position and cross section of the locally injected sodium in relation to the gas stream.

Sensibility

Sensibility may be checked while the pyrometer is operating with the specified sodium concentration in the gas. The system is displaced from balance position by manually rotating the balancing motor. Upon release, the system returns toward balance. An approach toward balance from both directions will produce a dead zone observable on the lamp ammeter. The temperature sensibility is one-half this dead zone.

Another method of sensibility measurement is to observe the shift in gas-temperature indication caused when one or more clean windows are inserted between the optical unit and the gas. This has the effect of lowering the apparent brightness of the radiation from the lamp by a fraction equal to the transmission factor τ of the windows. Differentiation of Planck's equation shows that this change in brightness corresponds to an apparent change ΔT_g in gas temperature given by $\Delta T_g = \lambda_d T_g^2(1 - \tau)/c_2$.

Denote by $\Delta T_g'$ the indicated gas-temperature change when the window is alternately inserted and removed. If $0 < \Delta T_g' < \Delta T_g$, the sensibility is given by $\frac{1}{2}(\Delta T_g - \Delta T_g')$. A typical clean window has a transmission factor of 0.92, yielding $\Delta T_g = 22^\circ$ R at $T_g = 3500^\circ$ R.

PERFORMANCE AND RESULTS

Tests were made in a tunnel by burning gasoline (ref. 6) and producing exhaust-gas flow through a concentric A.S.M.E. nozzle of 4-inch diameter. The tests covered the ranges $0.3 < M < 0.7$, $p \approx 1$ atmosphere, and $2900^\circ \text{ R} < T_g < 3900^\circ \text{ R}$.

Preliminary tests were concerned with the determination of some of the optical constants involved in the calibration, the operation of the powder injection method, and operation of the self-balancing system; final tests were concerned with an intercomparison of various D-line reversal measurements, and with a comparison of the D-line reversal pyrometer with a pneumatic-probe pyrometer and a thermocouple pyrometer.

Calibration Constants

The transmission factor of the optical unit, without tunnel window, was separately determined to be 0.474; the transmission factor of a 2-inch-thick, uncoated, fused quartz tunnel window was separately determined to be 0.923. Thus, the resultant value of τ_1 was 0.437. This value was used with figure 12 to provide the first correction to the optical-pyrometer reading.

The transmission factor of the reflector alone was separately determined to be 0.860; combined with the doubled transmission through another 2-inch-thick fused quartz window, the resultant transmission factor τ_3 was 0.733. From table II, with $\varepsilon_r = 0.50$, an average value of τ_3' is therefore 0.86. This value was used with figure 13 to provide a final correction to the optical-pyrometer reading.

Powder Injection Pattern

With the mouth of the powder-injecting probe located on the centerline of the nozzle exit and in the plane of the exit, where there was little turbulence, a cylindrical stream of yellow-colored gas of about 3/4-inch diameter was maintained at least 12 inches downstream of the injector at $0.3 < M < 0.9$.

With the mouth of the probe located in the mixing region downstream of the nozzle, a 15°-included-angle cone of sodium-containing gas was maintained for at least 12 inches from the injector.

After leaving the probe mouth, the powder required a distance of about 1 inch to reach maximum brightness. This was interpreted to be the distance that the powder required to vaporize and to reach an equilibrium temperature.

The required sodium bicarbonate powder injection rate was determined from equation (14) using the appropriate vapor-stream diameter.

Self-Balancing-System Operation

Unexpected defects of the self-balancing systems, or unusual causes such as ambient light from fluorescent lamps, may conceivably introduce an error of reversal determination. A general test for the presence of such an error was made before the heated gas was produced by verifying that there was no change in temperature indication for any lamp current within the temperature range of the instrument. Lamp current was varied using the knob on the electrical unit (fig. 1).

In the middle of the temperature range, temperatures varying at rates below 500° per second could be followed with a time lag of 1/4 second, with a sensibility of 10° R. Time to reach full scale was 3.0 seconds.

Sensibility and Temperature Limits

The sensibility as determined by insertion of clean glass windows between the optical unit and the adjacent window was 10° at temperatures above 3300° R and about 50° R at 3100° R. At gas temperatures below 2900° R, the D-line intensity was insufficient to drive the servomotor. Reversal could not be observed visually with a manually operated single-pass system below 2900° R.

The upper temperature limit of the instrument, 4500° R, is set by the temperature of 5550° R at which it is considered safe to operate the tungsten-filament lamp without excessively rapid change of calibration caused by vaporization of the filament and consequent blackening of the glass bulb.

Comparison of Self-Balancing and Manual Methods

For manual operation the reflector was replaced by a spectroscope, and the lamp voltage was controlled manually. In this method the gas was crossed by the light path only once. Lamp calibration for a single-pass system (eq. (7) and table I) was used, since the correction for the presence of the reflector was not applicable. A comparison of the self-balancing and manual operations is shown in figure 15 with the sodium injector probe located downstream of the tunnel nozzle, 4 inches upstream of the light path. The average random deviation was 20° R.

Tests were also made with two sodium injector probes, one located upstream and one located downstream of the tunnel nozzle, and with both probes in the gas at all times. Both probes gave the same indication.

Comparison with Other Types of Thermometers

Readings made on the same gas stream using the automatic D-line reversal pyrometer, a pneumatic-probe pyrometer, and a thermocouple pyrometer are compared in figure 16. No details will be given herein of these other pyrometers other than to say that the best technique possible was used, including the application of all known systematic corrections.

The agreement among the three instruments is believed to establish the upper limit of the possible inaccuracy of the D-line reversal instrument. Weighting all instruments equally, the average deviation of the D-line reversal instrument is 60° R.

Lewis Flight Propulsion Laboratory
National Advisory Committee for Aeronautics
Cleveland, Ohio, April 11, 1956

APPENDIX A

SYMBOLS

The following symbols are used in this report:

A	area of aperture
a	distance from center of sodium vapor stream to edge of gas stream
b	width of gas stream along light path
C	geometrical constant of spectroscope, $C = A\omega$
C_1	sodium-injection-rate constant, 5.9×10^{-6} lb atm in.$^{-1}$ sec^{-1}
C_2	sodium-injection-rate constant, 1.38×10^{-8} lb atm^{-1} in.$^{-1}$ sec^{-1}
C_3	Doppler line-width constant, $6.68\times10^{-4}\ A(^{\circ}R)^{-\frac{1}{2}}$
C_4	collision line-width constant, $5.03\ A(^{\circ}R)^{1/2}$ atm^{-1}
C_5	Doppler absorption-coefficient constant, 1.225×10^{-22} in.^{3} for 5896 A; 2.45×10^{-22} in.^{3} for 5890 A
C_6	lifetime of sodium atom in resonance state, 1.5×10^{-6} sec
C_7	sodium-injection-rate constant, 1.93×10^{19} atm in.$^{-1}$ sec^{-1}
C_8	sodium-injection-rate constant, 4.5×10^{16} atm^{-1} in.$^{-1}$ sec^{-1}
c	velocity of light in vacuo
c_1	Planck's radiation constant, 0.58×10^{-12} watt-in.^{2}
c_2	Planck's radiation constant, 1.016 in. $^{\circ}R$
Δf	frequency band width
g_2/g_1	constant, 1.0 at 5896 A; 2.0 at 5890 A
i	photocell current due to radiant flux

i_{dc} photocell direct current due to light flux

i_n photocell noise current

i_s photocell signal current

i_t photocell thermionic current

k radiation absorption coefficient

M Mach number

N monochromatic areal intensity

$\mathcal{N}$ number of sodium atoms per unit volume

$\mathcal{N}_c$ number of sodium atoms per unit mass of compound

n refractive index

p gas static pressure, atm

R specific gas constant for dry air, 1718 sq ft/(sec^2)($^\circ$R)

T temperature of object

T_b' temperature of blackbody producing, at average wavelength $\lambda = \lambda_d$ (5893 A), the same monochromatic areal intensity at the gas location as that produced by the lamp

T_b'' temperature of blackbody producing, at wavelength $\lambda = \lambda_v$ (6650 A), the same areal intensity at the gas location as that produced by the lamp

t gas transmission variable

u linear velocity of gas stream

w mass flow rate of sodium compound

y length of light path through sodium vapor stream

α	absorptivity
γ	ratio of specific heats for flame gases, 1.25
ε	emissivity
ε_r	effective emissivity for line reversal
λ	wavelength of radiation
$\Delta\lambda$	wavelength interval transmitted by spectroscope slit S_3, or spectral-line width at half-maximum
$\lambda_{1,2,3,4}$	wavelengths defined in fig. 3
μ	photocell sensitivity, output current/incident power
ρ	reflectivity of lamp filament
τ	optical transmission factor
τ_1	transmission factor of optics between lamp filament and gas
τ_1'	modifying factor of τ_1 due to lamp-filament reflection
τ_1''	modifying factor of τ_1 due to particles in gas
τ_2	transmission factor of optics between gas and photocell
τ_3	transmission factor of optics between gas-reflector-gas
τ_3'	modifying factor of τ_3 due to presence of reflector
τ_3''	modifying factor of τ_3 due to particles in gas
τ_4	transmission factor of color filter
τ^*	loop transmission factor of double-pass system without gas absorption
τ^{**}	loop transmission factor of double-pass system with gas absorption
φ	radiant flux
ω	solid angle of radiation subtended about area A

Subscripts:

a	air
av	average
b	blackbody
c	center wavelength of assumed C-line
D	Doppler effect
d	center wavelength of assumed D-line
e	center wavelength of assumed E-line
g	gas
gl	glass
h	fictitious center wavelength
L	collision of atoms (Lorentz broadening)
l	lamp
p	solid particle in gas stream
t	total effect of Doppler, Lorentz, and absorption broadening
v	red color radiation at 6650 A of optical pyrometer
λ	wavelength
0	reference value, center wavelength of spectral line

APPENDIX B

REVERSAL EQUATION

Single-Pass System

The reversal equation is to be written in terms of the light fluxes transmitted by slit S_3 at λ_c, λ_d, and λ_e, and the corresponding photocell currents. It is assumed that the sensitivity of the observing apparatus may be different at λ_c, λ_d, and λ_e, and also that the wavelength intervals $\Delta\lambda_c$, $\Delta\lambda_d$, and $\Delta\lambda_e$ may be different because of a nonconstant dispersion of the spectroscope. The gas is assumed nonluminous before sodium is added. The gas emissivity $\varepsilon_{d,g}$ is assumed to be an arbitrary, continuously variable function of wavelength $\varepsilon = \varepsilon(\lambda)$ within the interval λ_2 to λ_3. Kirchoff's law is applied. A color filter τ_4 is included. The components of light flux are shown in figure 5. The light flux at λ_d slit position is

$$\varphi_d = C\tau_2\tau_{d,4}\left[\tau_1\varepsilon_{d,1}N_{d,1}\int_{\lambda_2}^{\lambda_3}(1-\varepsilon_{d,g})d\lambda + N_{d,g}\int_{\lambda_2}^{\lambda_3}\varepsilon_{d,g}d\lambda + \tau_1^2\rho_1 N_{d,g}\int_{\lambda_2}^{\lambda_3}\varepsilon_{d,g}(1-\varepsilon_{d,g})d\lambda\right] \quad (B1)$$

where $\alpha_g = \varepsilon_g$ by Kirchoff's law. At λ_c slit position,

$$\varphi_c = C\tau_1\tau_2\tau_{c,4}\varepsilon_{c,1}N_{c,1}\Delta\lambda_c \quad (B2)$$

At λ_e slit position,

$$\varphi_e = C\tau_1\tau_2\tau_{e,4}\varepsilon_{e,1}N_{e,1}\Delta\lambda_e \quad (B3)$$

The photocell current i_λ due to flux φ_λ is $i_\lambda = \mu_\lambda\varphi_\lambda$, where μ_λ represents the photocell circuit sensitivity (output current per unit radiant flux) at wavelength λ. The change in photocell current when the slit moves from the d-position to the e-position is

$$i_e - i_d = \mu_e\varphi_e - \mu_d\varphi_d \quad (B4)$$

The change in photocell current when the slit moves from the d-position to the c-position is

$$i_c - i_d = \mu_c\varphi_c - \mu_d\varphi_d \tag{B5}$$

The resultant current, after passing through the transformer, produces a signal that has both 60- and 120-cps components. The 60-cps component is represented, in peak-to-peak value, by the difference

$$(i_e - i_d) - (i_c - i_d) = \mu_e\varphi_e - \mu_c\varphi_c \tag{B6}$$

Although this current does not affect the balance point (which is different only on 120-cps components), it may nevertheless be large enough to partially block the amplifier and hence to introduce an undesirably large dead zone. This 60-cps current can be almost eliminated by choosing the color filter τ_4 so that, over the temperature range of interest, $\mu_e\varphi_e = \mu_c\varphi_c$ or, using equations (B2) and (B3),

$$\frac{\tau_{c,4}}{\tau_{e,4}} = \frac{\mu_e}{\mu_c}\frac{\Delta\lambda_e}{\Delta\lambda_c}\left(\frac{\varepsilon_{e,l}N_{e,l}}{\varepsilon_{c,l}N_{c,l}}\right)_{av} \tag{B7}$$

The 120-cps current is represented by the sum $\frac{1}{2}\left[(i_e - i_d) + (i_c - i_d)\right]$. This component operates the self-balancing system to reduce the sum to zero. Then,

$$(i_e - i_d) + (i_c - i_d) = 0 = -2\mu_d\varphi_d + \mu_e\varphi_e + \mu_c\varphi_c \tag{B8}$$

or, substituting equations (B1) to (B3),

$$\begin{aligned}(i_e - i_d) + (i_c - i_d) &= 0 \\ &= \left(c\mu_d\tau_2\tau_{d,4}\int_{\lambda_2}^{\lambda_3}\varepsilon_{d,g}\,d\lambda\right)\left[\tau_1\varepsilon_{d,l}N_{d,l} - N_{d,g} - \tau_1^2\rho_l(1 - \varepsilon_r)N_{d,g} + \right. \\ &\quad \left.\frac{\tau_1\varepsilon_{d,l}N_{d,l}\Delta\lambda_d}{\int_{\lambda_2}^{\lambda_3}\varepsilon_{d,g}\,d\lambda}\left(\frac{\mu_e\tau_{e,4}\varepsilon_{e,l}N_{e,l}\Delta\lambda_e + \mu_c\tau_{c,4}\varepsilon_{c,l}N_{c,l}\Delta\lambda_c}{2\mu_d\tau_{d,4}\varepsilon_{d,l}N_{d,l}\Delta\lambda_d} - 1\right)\right]\end{aligned} \tag{B9}$$

where the last term can be designated $\Delta N_{d,l}$, and an effective emissivity ε_r is defined as

$$\varepsilon_r \equiv \frac{\int_{\lambda_2}^{\lambda_3} \varepsilon_{d,g}^2 \, d\lambda}{\int_{\lambda_2}^{\lambda_3} \varepsilon_{d,g} \, d\lambda} \tag{B10}$$

The effective emissivity ε_r may be measured by the following procedure based on a comparison of single-pass and double-pass measurements (refs. 7 and 8). The lamp is turned off, and a black card is placed on the optical axis next to the lamp to eliminate the factor τ^*. Sodium is injected at the specified rate. The photocell alternating-current output is measured (slit S_3 in motion)

(1) With the reflector in place, yielding a current i_2 for a doubled-path length through the gas.

(2) With the reflector and its window covered by a shutter, yielding a current i_1 for a single-path length through the gas.

(3) With the window next to the optical unit and covered by a shutter, yielding a dark current i_3. The emissivity is calculated from the following equation:

$$\varepsilon_r = \frac{1}{\tau_3}\left[1 + \tau_3 - \left(\frac{i_2 - i_3}{i_1 - i_3}\right)\right] \tag{B11}$$

It is necessary to maintain a constant gas temperature and sodium injection rate while currents i_2 and i_1 are measured.

Double-Pass System

In the analysis without reflector, three center wavelengths λ_c, λ_d, and λ_e were used to derive the reversal equation. In the analysis, the errors of the self-balancing system were pointed out. These errors have been substantially eliminated (by use of an appropriate color filter and an appropriately phased electric bucking voltage); so it is now possible to study the conditions with a reflector by assuming the following conditions:

$$\mu_c + \mu_e = 2\mu_d = 2\mu_h$$

$$\tau_{c,4} + \tau_{e,4} = 2\tau_{d,4} = 2\tau_{h,4}$$

$$\varepsilon_{c,l} + \varepsilon_{e,l} = 2\varepsilon_{d,l} = 2\varepsilon_{h,l}$$

$$N_{c,l} + N_{e,l} = 2N_{d,l} = 2N_{h,l}$$

$$\Delta\lambda_c + \Delta\lambda_e = 2\Delta\lambda_d = 2\Delta\lambda_h$$

and

$$N_{c,g} + N_{e,g} = 2N_{d,g} = 2N_{h,g}$$

where, for convenience, the two subscripts c and e are replaced by one common subscript h. This condition simplifies development of a reversal equation for the two-pass system.

During operation with the reflector in place, a part of the light reflected back to the optical unit of figure 2 is transmitted through the splitter plate to the lamp filament, where a fraction ρ_l is reflected. This reflection occurs for both the gas radiation and the lamp radiation; its effect is to increase the magnitude of the light-flux components used in deriving the reversal equations for the case of no reflector. The areal intensity of each component is multiplied by $\frac{1}{1 - \rho_l \tau_1^2 \tau_3}$ when there is no gas absorption and by $\frac{1}{1 - \rho_l \tau_1^2 \tau_3 (1 - \varepsilon_{\lambda,g})^2}$ when there is gas absorption. The second terms of the denominator in the preceding expressions may be considered to be "loop transmission factors"; they will be designated by

$$\tau^* \equiv \rho_l \tau_1^2 \tau_3 \tag{B12}$$

$$\tau^{**} = \rho_l \tau_1^2 \tau_3 (1 - \varepsilon_{\lambda,g})^2 \tag{B13}$$

The emissivity $\varepsilon_{d,g}$ will be assumed to be an arbitrary, continuously variable function of wavelength, $\varepsilon = \varepsilon(\lambda)$.

At the D-line λ_d (fig. 6),

$$\varphi_d = C\tau_2\tau_{d,4}\left[\tau_1\tau_3\varepsilon_{d,l}N_{d,l}\int_{\lambda_2}^{\lambda_3}\frac{(1 - \varepsilon_{d,g})^2}{1 - \tau_d^{**}}\,d\lambda + \tau_3 N_{d,g}\int_{\lambda_2}^{\lambda_3}\frac{\varepsilon_{d,g}(1 - \varepsilon_{d,g})}{1 - \tau_d^{**}}\,d\lambda + N_{d,g}\int_{\lambda_2}^{\lambda_3}\frac{\varepsilon_{d,g}}{1 - \tau_d^{**}}\,d\lambda\right] \tag{B14}$$

At λ_h with lamp variables $\varepsilon_{h,l}N_{h,l} = \varepsilon_{d,l}N_{d,l}$,

$$\varphi_h = C\tau_2\tau_{d,4}\left(\tau_1\tau_3\varepsilon_{d,l}N_{d,l}\int_{\lambda_2}^{\lambda_3}\frac{1}{1-\varepsilon^*}\,d\lambda\right) \tag{B15}$$

The peak-to-peak unbalance signal is a photocell current

$$i_h - i_d = \mu_d(\varphi_h - \varphi_d) \tag{B16}$$

where $\mu_h = \mu_d$. At reversal, as detected by the instrument, $i_h = i_d$; therefore,

$$\varphi_h = \varphi_d \tag{B17}$$

Substituting equations (B14) and (B15) in equation (B17) yields

$$N_{d,g}\int_{\lambda_2}^{\lambda_3}\frac{\tau_3\varepsilon_{d,g}(1-\varepsilon_{d,g})+\varepsilon_{d,g}}{1-\tau_d^{**}}\,d\lambda =$$

$$\tau_1\tau_3\varepsilon_{d,l}N_{d,l}\int_{\lambda_2}^{\lambda_3}\frac{1}{1-\tau^*}-\frac{(1-\varepsilon_{d,g})^2}{1-\tau_d^{**}}\,d\lambda \tag{B18}$$

The quantity $\frac{1}{1-\tau_d^{**}}$ is within 10 percent of unity for all values of $\varepsilon_{d,g}$ and can be treated as a constant and cancelled out. Let the ratio $\frac{1-\tau_d^{**}}{1-\tau^*} \approx 1+\tau^*-\tau_d^{**}$. Then, using equation (B13), equation (B18) becomes

$$\frac{N_{d,g}}{\tau_1\varepsilon_{d,l}N_{d,l}} = \tau_3\frac{(1+\tau^*)\displaystyle\int_{\lambda_2}^{\lambda_3}2\varepsilon_{d,g}-\varepsilon_{d,g}^2\,d\lambda}{\displaystyle\int_{\lambda_2}^{\lambda_3}(1+\tau_3)\varepsilon_{d,g}-\tau_3\varepsilon_{d,g}^2\,d\lambda} \tag{B19}$$

3797

Divide numerator and denominator by $\int_{\lambda_2}^{\lambda_3} \varepsilon_{d,g}\, d\lambda$. Substitute the effective emissivity ε_r (eq. (B10)) to yield the calibration equation

$$N_{d,g} = \tau_1 \varepsilon_{d,l} N_{d,l} \tau_3' \tag{B20}$$

where, from equation (B12),

$$\tau_3' = \tau_3 (1 + \rho_l \tau_1^2 \tau_3) \frac{2 - \varepsilon_r}{1 + \tau_3 (1 - \varepsilon_r)} \tag{B21}$$

APPENDIX C

CALIBRATION

Temperature Correction for Wavelength Shift

The lamp is calibrated with an optical pyrometer that compares the brightness of the lamp with the brightness of an internal reference standard in a narrow wavelength interval centered about 6650 A. If the lamp is at a temperature T_l, it will produce, at the gas location, yellow radiation of monochromatic areal intensity

$$\varepsilon_{d,l}\tau_l N_{d,l} = \varepsilon_{d,l}\tau_l c_1 \lambda_d^{-5} e^{-\frac{c_2}{\lambda_d T_l}} \tag{C1}$$

and red radiation of monochromatic areal intensity

$$\varepsilon_{v,l}\tau_l N_{v,l} = \varepsilon_{v,l}\tau_l c_1 \lambda_v^{-5} e^{-\frac{c_2}{\lambda_v T_l}} \tag{C2}$$

The optical pyrometer at the gas location, when focused upon the lamp, gives only the equivalent blackbody temperature T_b'' at the gas location for red radiation for which

$$\varepsilon_{v,l}\tau_l N_{v,l} = c_1 \lambda_v^{-5} e^{-\frac{c_2}{\lambda_v T_b''}} \tag{C3}$$

Therefore the equivalent blackbody temperature T_b' at the gas location for yellow radiation for which

$$\varepsilon_{d,l}\tau_l N_{d,l} = c_1 \lambda_d^{-5} e^{-\frac{c_2}{\lambda_d T_b'}} \tag{C4}$$

has to be found. Elimination of T_l from equations (C1) to (C4) yields

$$\frac{1}{T_b'} - \frac{1}{T_b''} = \frac{\lambda_v \ln \varepsilon_{v,l} - \lambda_d \ln \varepsilon_{d,l} + (\lambda_v - \lambda_d)\ln \tau_l}{c_2} \tag{C5}$$

The difference between T_b' and T_b'' depends mainly upon the deviation of $\varepsilon_{v,l}$ and $\varepsilon_{d,l}$ from unity. The difference between T_b' and T_b'' could exist even if the emissivities $\varepsilon_{v,l}$ and $\varepsilon_{d,l}$ were equal.

Assuming values of $\varepsilon_{v,l}$ and $\varepsilon_{d,l}$ from data given in reference 9 (appendix II, p. 496), figure 12 has been prepared to provide the correction $T_b' - T_b''$ for wavelength shift when the optical pyrometer reading T_b'' and the transmission factor τ_1 are given. The lamp filament temperature of 5100° F shown in this figure is the maximum at which it is considered safe to operate the lamp without excessively rapid change of calibration.

Determination of Transmission Factors τ_1 and τ_3

The determination of τ_1 and τ_3 is made with the optical pyrometer. Let T_1 represent the pyrometer indication when the pyrometer is focused on the lamp filament, sighting through only the glass bulb. Let T_2 represent the pyrometer indication when the pyrometer is focused on the lamp filament, sighting back through the window of the optical unit plus one window added to represent the lamp bulb. Then τ of the optical-unit projection system including the lamp bulb is

$$\tau = e^{-\frac{c_2}{\lambda_v}\left(\frac{1}{T_2} - \frac{1}{T_1}\right)} \tag{C6}$$

The determination can be performed at any convenient temperature. Equation (C6) can be used to determine the transmission factor of each of the glass elements used with the instrument. Then τ_1 and τ_3 can be calculated from the transmission products:

$$\tau_1 = (\tau_{\text{tunnel window}})(\tau_{\text{optical-unit projection system}})$$

$$\tau_3 = (\tau^2_{\text{tunnel window}})(\tau_{\text{reflector}})$$

Determination of Transmission Factor τ_3'

The value of τ_3' is obtainable from table II with either a median value $\varepsilon_r = 0.5$ or a measured ε_r using equation (B11).

Determination of Gas Temperature T_g

By Wien's equation, the monochromatic areal intensity $N_{d,g}$ is related to the gas temperature T_g by

$$N_{d,g} = c_1 \lambda_d^{-5} e^{-\frac{c_2}{\lambda_d T_g}} \tag{C7}$$

Combination of equation (C7) with equations (C4) and (7) or (10) allows introduction of the constant τ:

$$\frac{1}{T_g} = \frac{1}{T_b'} - \frac{\lambda_d}{c_2} \ln \tau \tag{C8}$$

where τ can be τ_1' or τ_3', as well as $\tau_1'\tau_1''$ or $\tau_3'\tau_3''$ for a luminous gas of appendix E. Figure 13 has been prepared to provide the correction $T_g - T_b'$ for transmission factors when T_b' and τ are given. Thus, the gas temperature for the double-pass system is obtainable from the tabulation of the optical-pyrometer reading T_b'' against lamp current, figure 12, table II, and figure 13. Table IV shows these steps in the lamp calibration.

APPENDIX D

SODIUM INJECTION

Rate of Sodium Injection

Assume that a sodium compound is injected into the gas forming a stream of sodium-containing vapor of circular cross section with diameter y. Let $\mathcal{N}_c$ represent the number of sodium atoms contained in a unit mass of the injected compound; let $\mathcal{N}$ represent the number of sodium atoms per unit volume of the vapor stream. Then the required rate of mass flow w of a compound for two traverses by the light beam is

$$w = \frac{1}{2}\left(\frac{\mathcal{N}}{\mathcal{N}_c}\frac{u\pi y^2}{4}\right) = \frac{\pi(\mathcal{N}y)uy}{8\mathcal{N}_c} \tag{D1}$$

where u is the linear velocity of the gas stream. The velocity u is given in terms of the gas static temperature T and Mach number as

$$u = M\sqrt{\gamma RT} \tag{D2}$$

where γ is the ratio of specific heats and R is the specific gas constant.

The quantity $\mathcal{N}y$ in equation (D1) is proportional to the "optical depth" of the sodium atoms, which determines the ultimate width and shape of the D-line. In this report a criterion was chosen for a sodium injection rate sufficient to produce a D-line absorptivity of 0.5 at wavelengths 0.5 A from each side of the center wavelength λ_0. A relation between $\mathcal{N}y$ and this criterion will be developed in the following section.

Spectral-Line Width and Shape

The initial absorption-line width is predominantly determined by Doppler and collision processes; natural damping and hyperfine structure will be neglected. The absorption line half-maximum width caused by the Doppler effect is given, using equation (33) of reference 10, as

$$\Delta\lambda_D = C_3\sqrt{T} \tag{D3}$$

where

$$C_3 = 6.55\times10^{-4}\ A(^\circ R)^{-\frac{1}{2}}$$

The absorption-line half-maximum width caused by collision of atoms in flame gases is given, using equation (104) of reference 10, as

$$\Delta\lambda_L = C_4 \, p/\sqrt{T} \tag{D4}$$

where

$$C_4 = 2.98 \, A(^{\circ}R)^{\frac{1}{2}} \, atm^{-1}$$

using a gas molecular weight of 28 and an effective cross section of 64×10^{-16} A^2.

The shape of an absorption line, illustrated in figure 14, is given by equation (20) of reference 10:

$$N_\lambda = N_0 e^{-k_\lambda y} = N_0(1 - \alpha_\lambda) \tag{D5}$$

where $k_\lambda y$ is the "optical depth," and k_λ is the absorption coefficient. Substitution of a function $k = k(\lambda)$ in equation (D5) can determine the particular shape of a line. Both Doppler and collision effects are of interest.

The absorption coefficient due to the Doppler effect is obtained from equation (32) of reference 10:

$$k_{\lambda,D} = k_{0,D} \exp - \left[\frac{2(\lambda - \lambda_0)}{\Delta\lambda_D} \sqrt{\ln 2}\right]^2$$

The absorption coefficient due to the collision effect is obtained from equation (92) of reference 10:

$$k_{\lambda,L} = k_{0,L} \frac{1}{1 + \left[\frac{2(\lambda - \lambda_0)}{\Delta\lambda_L}\right]^2}$$

The absorption coefficient when both Doppler and collision effects are present is obtained from equation (94) of reference 10:

$$\frac{k_{\lambda,D,L}}{k_{0,D}} = \frac{2}{\pi\Delta\lambda_L} \int_{-\infty}^{\infty} \frac{\exp - \left[\frac{2\delta}{\Delta\lambda_D} \sqrt{\ln 2}\right]^2}{1 + \left[\frac{2}{\Delta\lambda_L} (\lambda - \lambda_0 - \delta)\right]^2} \, d\delta \tag{D6}$$

where δ is a variable of integration. In this equation the interdependence of Doppler and collision broadening is neglected. The integration has been done by various techniques (e.g., ref. 11), and some values are given in table IX of reference 10. An independent equation will now be derived for the ratio $k_{\lambda,D,L}/k_{0,D}$ in terms of $\mathcal{N}y$.

The Doppler absorption coefficient $k_{0,D}$ in equation (D6) is, using equation (35) of reference 10,

$$k_{0,D} = C_5\sqrt{\frac{\ln 2}{\pi}}\frac{\mathcal{N}}{\Delta\lambda_D} \tag{D7}$$

where

$$C_5 = \frac{\lambda_0^4}{4\pi c\, C_6}\frac{g_2}{g_1}$$

$$= 1.225\times10^{-22} \text{ in.}^3 \quad \text{for 5896 A}$$

$$= 2.45\times10^{-22} \text{ in.}^3 \quad \text{for 5890 A}$$

For the absorptivity criterion that $\alpha_{\lambda,g} = 0.5$ at $\lambda - \lambda_0 = 0.5$ A, as specified in this report,

$$\alpha_{\lambda,g} = 1 - e^{-k_{\lambda,D,L}y} = 0.5$$

or

$$k_{\lambda,D,L} = \frac{\ln 2}{y} \tag{D8}$$

where $\lambda - \lambda_0 = 0.5$ A. Combining equations (D7) and (D8) yields

$$\mathcal{N}y = \frac{\sqrt{\pi \ln 2}\,\Delta\lambda_D}{C_5}\left(\frac{1}{k_{\lambda,D,L}/k_{0,D}}\right) \tag{D9}$$

Thus, the quantity $\mathcal{N}y$ depends upon the initial width $\Delta\lambda_D$ and equation (D6). Equation (D9) is plotted in figure 17 for a temperature of 3700° R, for a D-line at a wavelength of 5896 A, for $2(\lambda - \lambda_0) = 0.5$, 1.0, or 2.0 A, and the solution of equation (D6). For the other D-line at a wavelength of 5890 A, the sodium concentration would be halved because C_5 is doubled. In figure 17 $\mathcal{N}y$ is a minimum at a pressure corresponding to $2(\lambda - \lambda_0) \approx \Delta\lambda_L$.

By using the curve for $2(\lambda - \lambda_0) = 1$ A in figure 17 with equations (D1) and (D2), the flow rate of a sodium compound is

$$w \approx C_7 \frac{My}{\mathcal{N}_c p} \qquad p < 20 \text{ atm}$$

$$w \approx C_8 \frac{Myp}{\mathcal{N}_c} \qquad p > 20 \text{ atm} \tag{D10}$$

where

$C_7 = 1.93 \times 10^{19}$ atm in.$^{-1}$ sec^{-1}

$C_8 = 4.5 \times 10^{16}$ atm^{-1} in.$^{-1}$ sec^{-1}

and the gas temperature is 3700° R. The value of w for a gas temperature of 3700° R is sufficiently accurate over the temperature range of the instrument.

The absorption coefficient $k_{0,D,L}$ per centimeter depth of gas has been experimentally determined in reference 12 to be about $1.5 \times 10^{-13}\mathcal{N}$. Gas temperature, pressure, and the D-line wavelength are not stated. This experimental value compares with the calculated value using equation (D7) and the solution of equation (D6) when $\lambda - \lambda_0 = 0$. For a wavelength of 5890 A, a gas temperature of 3700° R, and a pressure of 1 atmosphere, equations (D6) and (D7) yield $k_{0,D,L} = 1.3 \times 10^{-12}\mathcal{N}$ per centimeter.

APPENDIX E

GAS CONTAMINATION BY SOLID PARTICLES

In the analyses with and without reflector, the gas was assumed uncontaminated by solid materials. In practice the gas may contain small luminous particles, such as carbon, or larger particles of foreign material. The particles may not be at the gas temperature, and in some cases they may be cool enough to be nonluminous.

Unlike the sodium atom, a solid particle may scatter and reflect a significant fraction of the light incident upon it, depending upon its diameter. Thus, an incident-light beam transmitted by a cloud of particles suffers an attenuation along the direction of incidence, depending upon the particle diameter, absorptivity of the particle material, and particle concentration in the gas. To the instrument this cloud of particles will seem to have an absorptivity equal to the preceding attenuation. The emissivity will be assumed equal to this absorptivity.

The particle cloud produces mean values $N_{d,p,0}$ and $\varepsilon_{d,p,0}$ that represent the whole gas cross section; the mean value is designated by the subscript 0 (fig. 18(a)). Emissivity $\varepsilon_{d,p,0}$ will be considered independent of wavelength in the vicinity of the D-line. Only the condition of a low emissivity ($\varepsilon_{d,p,0} < 0.1$) will be considered. The monochromatic areal intensity $N_{d,g}$ represents the mean temperature of only that part of the gas bearing sodium vapor. Because of nonuniform gas temperature distribution, or the particles not at the gas temperature, $N_{d,g} \neq N_{d,p,0}$.

In figure 18(b) the radiated intensity from the gas stream is shown with sodium injected locally. A uniform distribution of the particles within the gas cross-section width b is assumed. Location of the injected sodium within the cross section is specified by the ratio a/b. With a reflector, the ratio a/b in gas stream 1 becomes a quantity $1 - a/b$ in the reflected image, gas stream 2.

Within the band width $\Delta\lambda_d$, the radiation is initiated by both the particles and the sodium atoms. If limiting values of a/b are considered ($a/b = 1.0$ and 0), the radiation intensity from streams 1 and 2 at slit position λ_d is

$$\left.\begin{aligned} N_1 &= A_1\varepsilon_{d,p,0}N_{d,p,0} + B_1\varepsilon_{d,g}N_{d,g} \\ N_2 &= A_2\varepsilon_{d,p,0}N_{d,p,0} + B_2\varepsilon_{d,g}N_{d,g} \end{aligned}\right\} \qquad (E1)$$

where

$$\left.\begin{aligned} A_1 &= 1 - \varepsilon_{d,g}\left(1 - \frac{a}{b}\right) \\ A_2 &= 1 - \varepsilon_{d,g}\frac{a}{b} \\ B_1 &= 1 - \varepsilon_{d,p,0}\frac{a}{b} \\ B_2 &= 1 - \varepsilon_{d,p,0}\left(1 - \frac{a}{b}\right) \end{aligned}\right\} \tag{E2}$$

The transmissivity at slit position λ_d is then

$$\left.\begin{aligned} t_1 &= 1 - A_1\varepsilon_{d,p,0} - B_1\varepsilon_{d,g} \\ t_2 &= 1 - A_2\varepsilon_{d,p,0} - B_2\varepsilon_{d,g} \end{aligned}\right\} \tag{E3}$$

For convenience, equations (E1) and (E3) can be rewritten using the new variable t as

$$\left.\begin{aligned} N_1 &= N_{d,g}\left[1 - t - \left(1 - \frac{N_{d,p,0}}{N_{d,g}}\right)(1 - t_0)\,A_1\right] \\ N_2 &= N_{d,g}\left[1 - t - \left(1 - \frac{N_{d,p,0}}{N_{d,g}}\right)(1 - t_0)\,A_2\right] \end{aligned}\right\} \tag{E4}$$

$$\left.\begin{aligned} t_0 &= 1 - \varepsilon_{d,p,0} \\ t &= t_1 = t_2 = t_0(1 - \varepsilon_{d,g}) \end{aligned}\right\} \tag{E5}$$

Equation (B13) then becomes

$$\left.\begin{aligned} \tau_h^{**} &= \tau^* t_0^2 \\ \tau_d^{**} &= \tau^* t^2 \end{aligned}\right\} \tag{E6}$$

These equations are used to write the light-flux components in figure 19.

At λ_d slit position,

$$\varphi_d = C\tau_2\tau_{d,4}\left\{\tau_1\tau_3\varepsilon_{d,l}N_{d,l}\int_{\lambda_2}^{\lambda_3}\frac{t^2}{1-\tau^*t^2}\,d\lambda + \tau_3N_{d,g}\int_{\lambda_2}^{\lambda_3}\frac{\left[1-t-\left(1-\frac{N_{d,p,0}}{N_{d,g}}\right)(1-t_0)A_2\right]t}{1-\tau^*t^2}\,d\lambda + N_{d,g}\int_{\lambda_2}^{\lambda_3}\frac{\left[1-t-\left(1-\frac{N_{d,p,0}}{N_{d,g}}\right)(1-t_0)A_1\right]}{1-\tau^*t^2}\,d\lambda\right\} \quad (E7)$$

At λ_h slit position with lamp variables $\varepsilon_{h,l} = \varepsilon_{d,l}$ and $N_{h,l} = N_{d,l}$,

$$\varphi_h = C\tau_2\tau_{d,4}\left\{\tau_1\tau_3\varepsilon_{d,l}N_{d,l}\int_{\lambda_2}^{\lambda_3}\frac{t_0^2}{1-\tau^*t_0^2}\,d\lambda + \tau_3N_{d,g}\int_{\lambda_2}^{\lambda_3}\left(\frac{N_{d,p,0}}{N_{d,g}}\right)\frac{t_0(1-t_0)}{1-\tau^*t_0^2}\,d\lambda + N_{d,g}\int_{\lambda_2}^{\lambda_3}\left(\frac{N_{d,p,0}}{N_{d,g}}\right)\frac{1-t_0}{1-\tau^*t_0^2}\,d\lambda\right\} \quad (E8)$$

The peak-to-peak unbalance signal current from the photocell is

$$i_h - i_d = \mu_d(\varphi_h - \varphi_d) \quad (E9)$$

where $\mu_h = \mu_d$. At reversal, as detected by the instrument, $i_h = i_d$; therefore,

$$\varphi_h = \varphi_d \quad (E10)$$

Substituting equations (E7) and (E8) in equation (E10) yields

$$N_{d,g}\int_{\lambda_2}^{\lambda_3}\left\{\frac{\tau_3\left[1 - t - \left(1 - \frac{N_{d,p,0}}{N_{d,g}}\right)(1 - t_0)A_2\right]t}{1 - \tau^* t^2} + \right.$$

$$\left.\frac{\left[1 - t - \left(1 - \frac{N_{d,p,0}}{N_{d,g}}\right)(1 - t_0)A_1\right]}{1 - \tau^* t^2} - \right.$$

$$\left.\tau_3\left(\frac{N_{d,p,0}}{N_{d,g}}\right)\frac{t_0(1 - t_0)}{1 - \tau^* t_0^2} - \left(\frac{N_{d,p,0}}{N_{d,g}}\right)\frac{1 - t_0}{1 - \tau^* t_0^2}\right\}d\lambda$$

$$= \tau_1\tau_3\varepsilon_{d,l}N_{d,l}\int_{\lambda_2}^{\lambda_3}\left(\frac{t_0^2}{1 - \tau^* t_0^2} - \frac{t^2}{1 - \tau^* t^2}\right)d\lambda \quad (E11)$$

The quantities $1/(1 - \tau^* t_0^2)$ and $1/(1 - \tau^* t^2)$ are within 10 percent of unity for all values of ε_g and can be treated as constant and cancelled out. Let the ratio $(1 - \tau^* t^2)/(1 - \tau^* t_0^2)$ be approximated by $1 + \tau^*(t_0^2 - t^2)$. Then equation (E11) becomes

$$N_{d,g}\int_{\lambda_2}^{\lambda_3}\left\{(\tau_3 t + 1)(1 - t) - \right.$$

$$(1 - t_0)\left[(\tau_3 t A_2 + A_1)\left(1 - \frac{N_{d,p,0}}{N_{d,g}}\right) + (\tau_3 t_0 + 1)\left(\frac{N_{d,p,0}}{N_{d,g}}\right)\right] -$$

$$\left.(1 - t_0)\tau^*(t_0^2 - t^2)(\tau_3 t_0 + 1)\left(\frac{N_{d,p,0}}{N_{d,g}}\right)\right\}d\lambda$$

$$= \tau_1\tau_3\varepsilon_{d,l}N_{d,l}(1 + \tau^* t_0^2)\int_{\lambda_2}^{\lambda_3}(t_0^2 - t^2)d\lambda \quad (E12)$$

The independent variable $\varepsilon_{d,g}$ appears only within the new variable t. Thus, the two terms in equation (E12) containing $t_0^2 - t^2$ can be combined. In this combined term, the approximation is made that

$N_{d,g} = \tau_1\tau_3\varepsilon_{d,l}N_{d,l}(1 - \tau^*t_0^2)$. That the approximation is good may be verified by inspection of equations (B20) and (B21); furthermore, the third term on the left side of the equation is small compared with all other terms because of the factors $1 - t_0$ and τ^*, which are much less than unity. Then equation (E12) becomes

$$N_{d,g}\int_{\lambda_2}^{\lambda_3}\left\{(\tau_3 t + 1)(1 - t) - (1 - t_0)\left[(\tau_3 t A_2 + A_1)\left(1 - \frac{N_{d,p,0}}{N_{d,g}}\right) + (\tau_3 t_0 + 1)\frac{N_{d,p,0}}{N_{d,g}}\right]\right\}d\lambda = \tau_1\tau_3\varepsilon_{d,l}N_{d,l}(1 - \tau^*t_0^2)\left[1 + (1 - t_0)\tau^*(\tau_3 t_0 + 1)\frac{N_{d,p,0}}{N_{d,g}}\right]\int_{\lambda_2}^{\lambda_3}(t_0^2 - t^2)d\lambda \quad \text{(E13)}$$

Replacing t, t_0, A_1, and A_2 by their equivalent expressions, equations (E2) and (E5), and dropping $\varepsilon_{d,p,0}^2$ (since $\varepsilon_{d,p,0} << 1.0$) yield

$$N_{d,g}\int_{\lambda_2}^{\lambda_3}\left[(\tau_3 + 1)\varepsilon_{d,g} - \tau_3\varepsilon_{d,g}^2\right] - \varepsilon_{d,p,0}\left\{\left[(3\tau_3 + 1) - \left(\tau_3 + 1 + \tau_3\frac{a}{b} - \frac{a}{b}\right)\left(1 - \frac{N_{d,p,0}}{N_{d,g}}\right)\right]\varepsilon_{d,g} - \left[2\tau_3 - \tau_3\frac{a}{b}\left(1 - \frac{N_{d,p,0}}{N_{d,g}}\right)\right]\varepsilon_{d,g}^2\right\}d\lambda = \tau_1\tau_3\varepsilon_{d,l}N_{d,l}(1 + \tau_h^*)\left[1 + \tau^*\varepsilon_{d,p,0}(\tau_3 + 1)\left(\frac{N_{d,p,0}}{N_{d,g}}\right)\right] \times \int_{\lambda_2}^{\lambda_3}(2\varepsilon_{d,g} - \varepsilon_{d,g}^2)(1 - 2\varepsilon_{d,p,0})d\lambda \quad \text{(E14)}$$

Divide both sides by $\int_{\lambda_2}^{\lambda_3}\varepsilon_{d,g}d\lambda$. Substitute the effective emissivity ε_r (eq. (B10)) to yield the equation in algebraic form:

$$N_{d,g} = \tau_1\varepsilon_{d,l}N_{d,l}\tau_3'\tau_3'' \quad \text{(E15)}$$

where τ'_3 is given by equation (11), and τ''_3, the luminous gas correction, is

$$\tau''_3 = 1 + \varepsilon_{d,p,0}\left\{\frac{\left[\frac{N_{d,p,0}}{N_{d,g}}\left(\tau_3 + 1 - \frac{a}{b}\right) + \frac{a}{b}\right] + \left[\left(\frac{N_{d,p,0}}{N_{d,g}} - 1\right)\frac{a}{b} + 2\right]\tau_3(1 - \varepsilon_r)}{1 + \tau_3(1 - \varepsilon_r)} + \tau^*\left(\frac{N_{d,p,0}}{N_{d,g}}\right)(\tau_3 + 1) - 2(1 + \tau^*)\right\} \quad \text{(E16)}$$

A similar equation for a single-pass optical system is

$$N_{d,g} = \tau_1 \varepsilon_{d,l} N_{d,l} \tau'_1 \tau''_1 \quad \text{(E17)}$$

where τ'_1 is given by equation (8), and τ''_1, the luminous gas correction, is

$$\tau''_1 = 1 + \varepsilon_{d,p,0}\left\{\frac{\left[\frac{N_{d,p,0}}{N_{d,g}}\left(\tau_1^2\rho_l + 1 - \frac{a}{b}\right) + \frac{a}{b}\right] + \left[\left(\frac{N_{d,p,0}}{N_{d,g}} - 1\right)\frac{a}{b} + 2\right]\tau_1^2\rho_l(1 - \varepsilon_r)}{1 + \tau_1^2\rho_l(1 - \varepsilon_r)} - 1\right\} \quad \text{(E18)}$$

in which the ratio a/b is defined by gas stream 1 (fig. 18). The equations are much simpler for an idealized case. Let the constants of equation (E16) be $a/b = 1.0$, $\tau_3 = 1.0$, and $\tau^* = 0$; for equation (E18) let $\rho_l = 0$ and $a/b = 0$. Then,

$$\tau''_3 = \tau''_1 = 1 + \varepsilon_{d,p,0}\left(\frac{N_{d,p,0}}{N_{d,g}} - 1\right) \quad \text{(E19)}$$

A rule-of-thumb conclusion may be drawn from this equation. For example, if the mean gas temperature is less than the temperature at the region of local injection, τ'' is less than 1.0. The temperature correction corresponding to τ'' as given by figure 13 is negative, and the indicated temperature is too high.

The effective emissivity ε_r may be measured by the procedure of appendix B. Since $\varepsilon_{d,p,0}$ is independent of wavelength, its average

and effective values are equal. The values of $\varepsilon_{d,p,0}$ and $N_{d,p,0}/N_{d,g}$ may be measured by different methods depending upon whether the particle and gas temperatures are equal or unequal. A method valid for unequal particle and gas temperatures is the "Two-Path Method with Comparison Source" described in reference 2. This method is used in the pyrometer of reference 4.

Local sodium injection is not used. The reflector is removed, and an optical pyrometer is sighted on the particles and lamp as in calibration (single pass through gas). Let T_1 represent the pyrometer indication with gas flow and with the ribbon-filament lamp turned off. Let T_2 represent the pyrometer indication with gas flow and the lamp turned on. Let T_3 represent the pyrometer indication without gas flow and with the lamp turned on, using the same value of lamp current as for T_2. Temperature T_3 may be obtained from the lamp calibration data if appropriate correction is made for the presence of a tunnel window. Then,

$$\alpha_{v,p,0} = 1 - e^{-\frac{c_2}{\lambda_v}\left(\frac{1}{T_1} - \frac{1}{T_3}\right)} + e^{-\frac{c_2}{\lambda_v}\left(\frac{1}{T_2} - \frac{1}{T_3}\right)}$$

This method measures the absorptivity at the pyrometer wavelength of 6650 A. The particles are assumed to be gray-body radiators and, as previously stated, Kirchhoff's law is assumed. Then,

$$\varepsilon_{d,p,0} = \alpha_{v,p,0}$$

Let T_4 represent the local temperature determined by the line-reversal pyrometer with local sodium injection, before applying the correction for particles. Then $N_{d,p,0}/N_{d,g}$ is, approximately,

$$\frac{N_{d,p,0}}{N_{d,g}} = \frac{e^{-\frac{c_2}{\lambda_d}\left(\frac{1}{T_1} - \frac{1}{T_4}\right)}}{\varepsilon_{d,p,0}}$$

REFERENCES

1. Lewis, Bernard, and vol Elbe, Guenther: Flame Temperature. Temperature - Its Measurement and Control in Science and Industry. Reinhold Pub. Corp., 1941, pp. 707-719.

2. Broida, H. P.: Experimental Temperature Measurements in Flames and Hot Gases. Vol. II of Temperature - Its Measurement and Control in Science and Industry, Reinhold Pub. Corp., 1955, pp. 265-286.

3. Sectional Committee on Letter Symbols and Abreviations for Science and Industry: American Standard - Letter Symbols for Heat and Thermodynamics, Including Heat Flow. ASA Z10.4, pub. by A.S.M.E., 1943.

4. Millar, G. H., Winans, J. G., Uyehara, O. A., and Myers, P. S.: A Fast, Electro-Optical, Hot-Gas Pyrometer. Jour. Optical Soc. Am., vol. 43, no. 7, July 1953, pp. 609-617.

5. Engstrom, Ralph W.: Multiplier Photo-Tube Characteristics: Application to Low Light Levels. Jour. Optical Soc. Am., vol. 37, no. 6, June 1947, pp. 420-431.

6. Glawe, George E., and Shepard, Charles E.: Some Effects of Exposure to Exhaust-Gas Streams on Emmitance and Thermoelectric Power of Bare-Wire Platinum Rhodium - Platinum Thermocouples. NACA TN 3253, 1954.

7. Bundy, F. P.: Effect of Temperature Zones on the Measurement of Temperature by the Absolute Radiation Method in Which the Optical Depth is Determined by the L vs 2L Method. Tech. Memo. No. NYU-2, Proj. Squid, Rep. on Conf. Measurement of Temperatures of Pulsating Burning Gases, Apr. 1948, pp. 42-50.

8. Bundy, F. P., and Strong, H. M.: Measurement of Temperatures in Flames of Complex Structure by Resonance Line Radiation. III - From Absolute Intensity Measurements at High Resolution. Jour. Appl. Phys., vol. 25, no. 12, Dec. 1954, pp. 1531-1537.

9. Worthing, Archie G., and Halliday, David: Heat. John Wiley & Sons, Inc., 1948.

10. Mitchell, Allan C. G., and Zemansky, Mark W. (E.K. Rideal, ed.): Resonance Radiation and Excited Atoms. Cambridge Univ. Press, 1934.

11. Penner, S. S., and Kavanagh, R. W.: Radiation from Isolated Spectral Lines with Combined Doppler and Lorentz Broadening. Jour. Optical Soc. Am., vol. 43, no. 5, May 1953, pp. 385-388.

12. Bundy, F. P., Strong, H. M., and Gregg, A. B.: Measurement of Velocity and Pressure of Gases in Rocket Flames by Spectroscopic Methods. Jour. Appl. Phys., vol. 22, no. 8, Aug. 1951, pp. 1069-1077.

TABLE I. - VALUES OF τ_1'

ε_r	τ_1				
	0.30	0.40	0.65	0.75	0.85
0	0.95	0.92	0.81	0.76	0.71
.50	.98	.96	.89	.85	.83
.75	.99	.98	.94	.93	.91
1.00	1.00	1.00	1.00	1.00	1.00

TABLE II. - VALUES OF τ_3'

ε_r	τ_3									
	0.70		0.75		0.80		0.85		0.90	
	τ_1									
	0.3	0.4	0.3	0.4	0.3	0.4	0.3	0.4	0.3	0.4
0	0.85	0.88	0.89	0.92	0.93	0.95	0.96	0.99	0.99	1.03
.50	.81	.83	.85	.87	.89	.92	.93	.97	.98	1.01
.75	.77	.79	.82	.85	.87	.90	.92	.95	.96	1.00
1.00	.73	.75	.78	.80	.83	.86	.89	.92	.94	.98

TABLE III. - SPECIFICATION OF MAJOR OPTICAL COMPONENTS

Symbol	Specification
T_1	Reference lamp: ribbon filament; 6 v; 18 amp; G.E. Mazda Code 18A/T10/2P-6V; medium prefocus base; filament projected area, 2mm by 8mm
T_2	Alinement lamp: G.E. type 1493, 6 v
T_3	Photomultiplier: type 931-A
L_1	Achromat condensing lens: biconvex, 34-mm diam., 65-mm focal length
L_2	Achromat condensing lens: plano-convex, 2-in. diam., 5-in. focal length
L_3	Achromat objective lens: 31.2-mm diam., 131.4-mm focal length, Bausch and Lomb Cat. No. 61-21-11-023
L_4	Cylindrical surface objective lens: plano-convex, 1/4-in. diam., 7/16-in. focal length, cylinder axis horizontal
L_5	Condensing lens: plano-convex, 1/2-in. diam., 1-in. focal length
L_6	Achromat spectroscope lens: 32-mm diam., 230-mm focal length, Bausch and Lomb Cat. No. 71-21-35-022
L_7	Achromat eyepiece lens: 9/16-in. diam., $1\frac{1}{2}$-in. focal length
P_1	Splitter plate: $2\frac{1}{2}$ in. by $3\frac{1}{8}$ in. by 1/8 in.; flat to 1λ; coated for 30 percent reflection, 70 percent transmission; Liberty Mirror Division of Libbey-Owens-Ford Glass Co. coat No. 300
P_2	Light trap: black velvet, $1\frac{1}{8}$ in. by $2\frac{1}{2}$ in.
P_3	Light trap: window glass, $1\frac{1}{2}$ in. by $2\frac{1}{2}$ in. by 1/8 in., painted black on rear side
P_4	Window: $2\frac{5}{16}$-in. diam. by $\frac{3}{16}$ in., flat to $1/2\lambda$
P_5	Reflector: corner-cube prism type, 2-in. depth from apex to face, 90° angles ± 2 min., total reflecting surfaces flat to $1/4\lambda$, face is convex with 49-in. rad., BSC-2 glass
P_6	Mirror: $\frac{3}{4}$ in. by $1\frac{3}{16}$ in. by $\frac{1}{8}$ in., flat to $1/4\lambda$, aluminized
P_7	Mirror: 1/2 in. by 9/16 in. by 1/16 in., rhodium coated
P_8	Pellin-Broca type prism: $1\frac{3}{16}$-in. square aperture, DF-3 glass, reflecting surface flat to $1/4\lambda$, refracting surfaces flat to $1/2\lambda$

TABLE III. - Concluded. SPECIFICATION OF MAJOR OPTICAL COMPONENTS

Symbol	Specification
P_9	Splitter plate: $1\frac{3}{16}$-in. diam.; 1/16 in. thick; flat to $1/2\lambda$; coated for 22 percent reflection, 78 percent transmission at D-line; Liberty Mirror Division of Libbey-Owens-Ford Glass Co. coating type 90-430.
P_{10}	Mirror: 1 in. by $1\frac{11}{16}$ in. by 3/16 in., flat to $1/2\lambda$, aluminized
P_{11}	Color filter: Corning Glass Works Spec. No. 2-73, Code No. 2934, 1/3 stock thickness
S_1	Aperture: 3/16 in. high by 5/8 in. wide
S_{2a}	Slit: 0.002 in. high by 13/64 in. wide
S_{2b}	Slit: 0.045 in. wide by 1/4 in. high
S_3	Slit: 0.003 in. high by 1/4 in. wide; amplitude, 0.008 in. peak-to-peak motion; D-line separation, 0.002 in.

TABLE IV. - CALIBRATION OF LAMP

[$\varepsilon_r = 0.5$, $\tau_1 = 0.44$, $\tau_3 = 0.73$, $\tau_3' = 0.86$]

Lamp current, amp	Optical-pyrometer reading, T_b'', °F	Correction for ε_l and τ_1, $T_b' - T_b''$, °F	T_b', °F	Correction for τ_3', $T_g - T_b'$ °F	Calibration temperature, T_g	
					°F	°R
8.64	2190	38	2228	-25	2203	2663
9.44	2375	45	2420	-28	2392	2852
9.96	2485	49	2534	-31	2504	2964
10.72	2635	54	2689	-34	2655	3115
11.44	2760	59	2819	-37	2782	3242
12.04	2865	63	2928	-40	2888	3348
12.72	2970	67	3037	-43	2994	3454
13.40	3080	72	3152	-46	3106	3566
14.08	3170	76	3246	-48	3198	3658
15.00	3310	83	3393	-51	3342	3802
16.00	3445	89	3534	-55	3479	3939

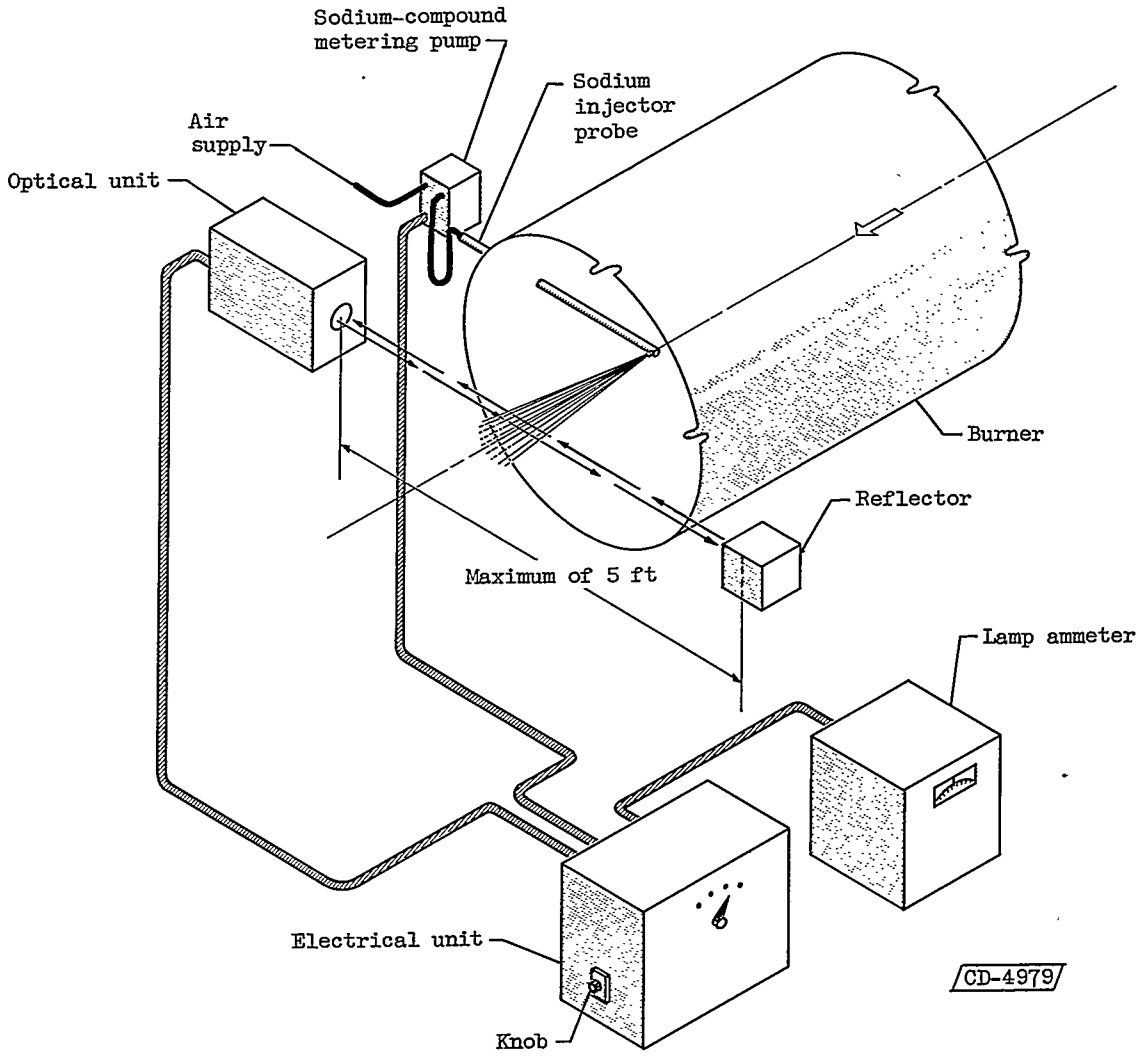

Figure 1. - Self-balancing line-reversal pyrometer.

CN-7 back 3797

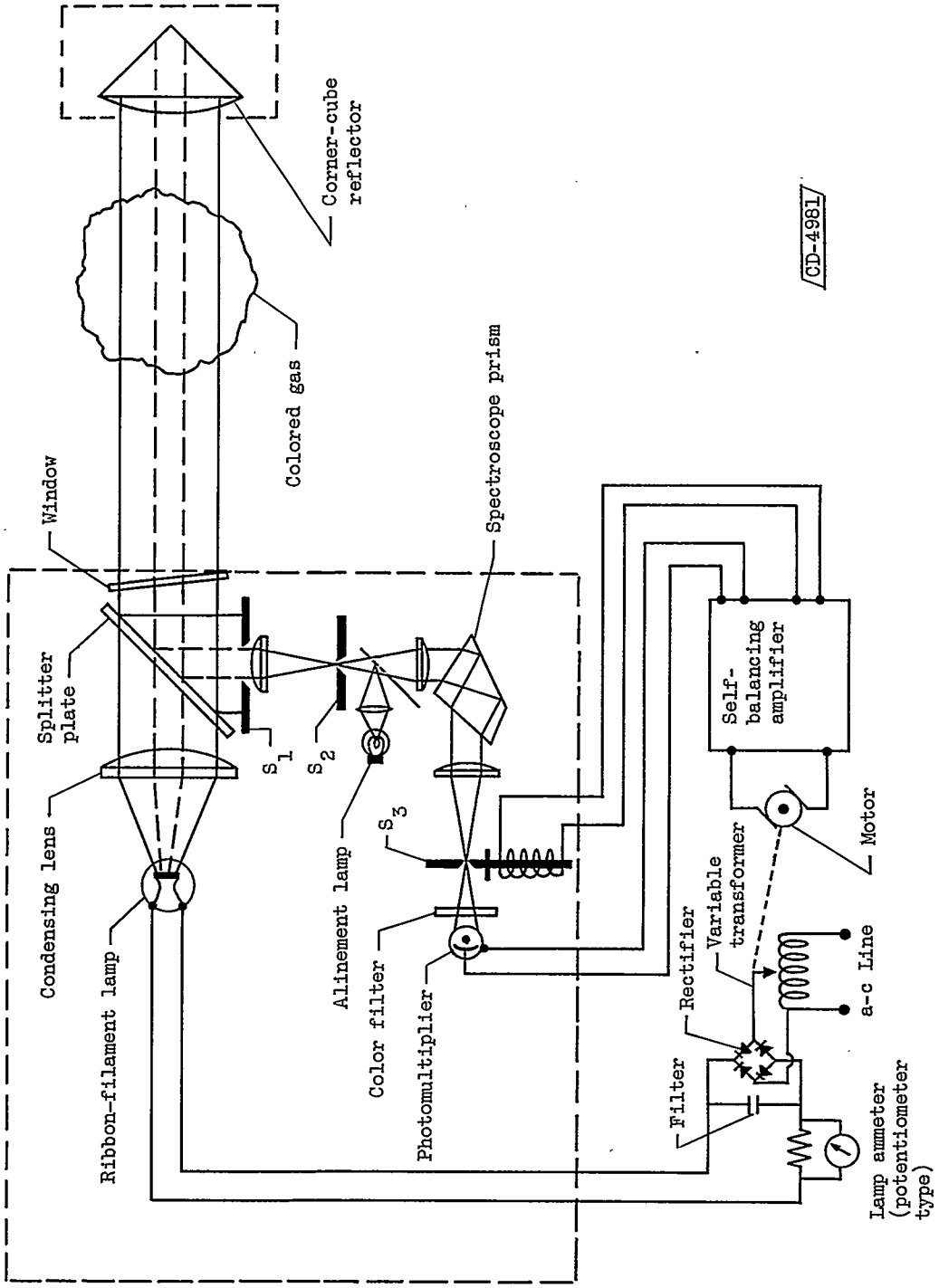

Figure 2. - Self-balancing method of line-reversal pyrometer.

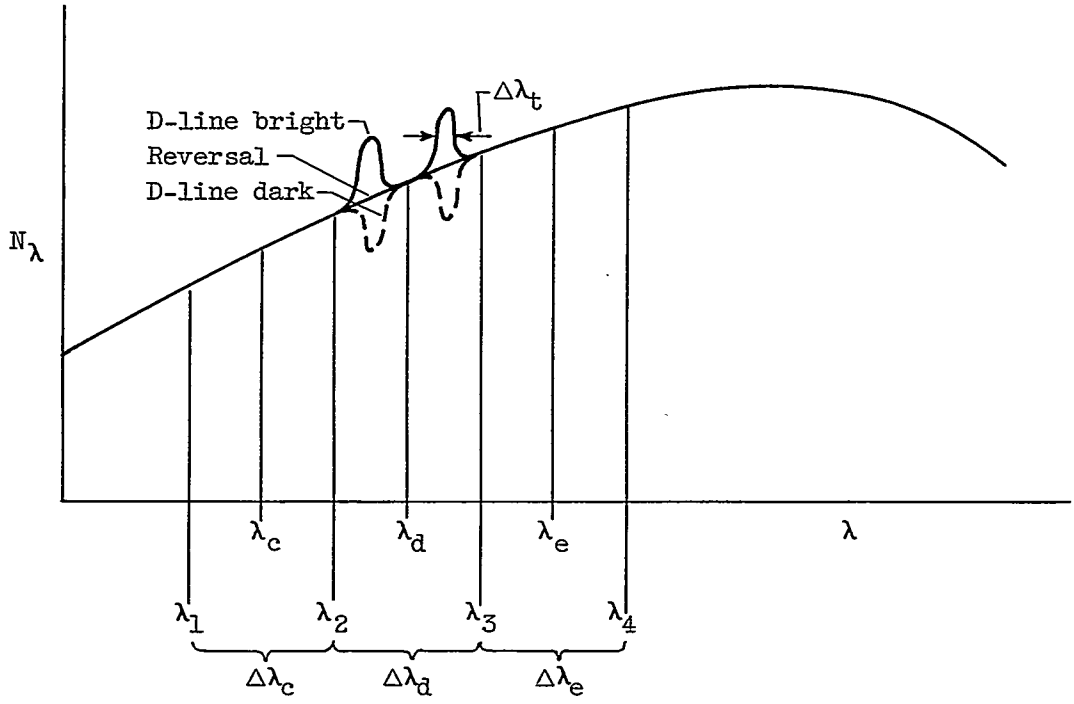

Figure 3. - Monochromatic areal intensity at spectroscope, with constant lamp temperature.

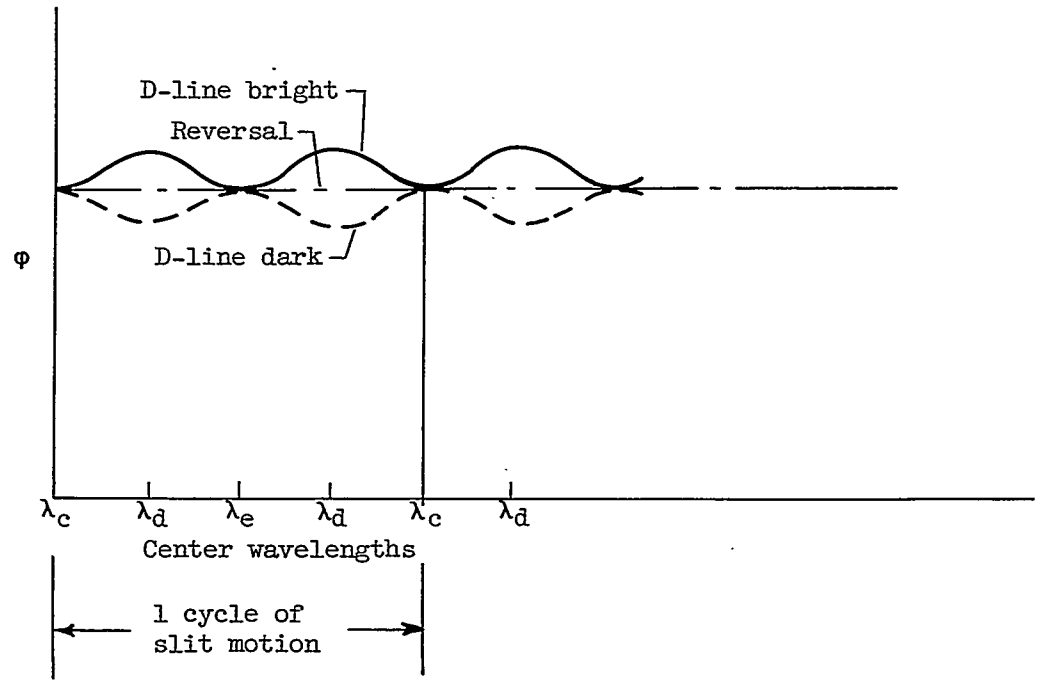

Figure 4. - Light flux transmitted by spectroscope slit.

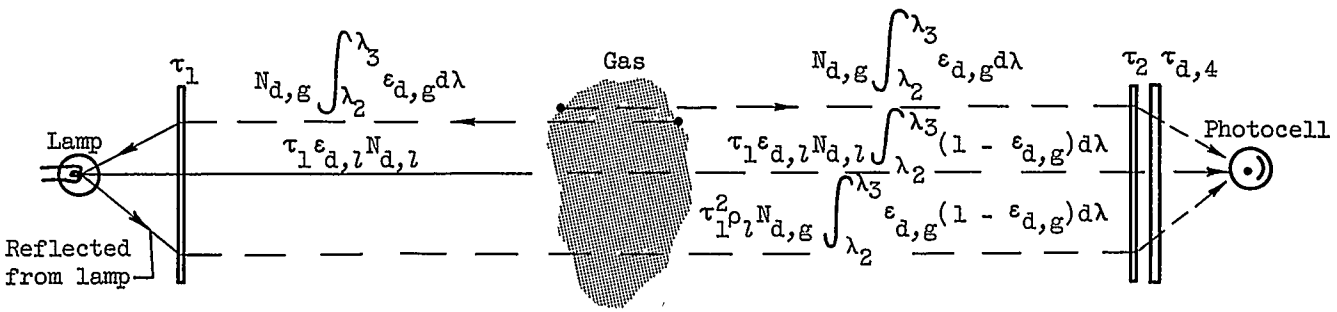

(a) Slit position, λ_d.

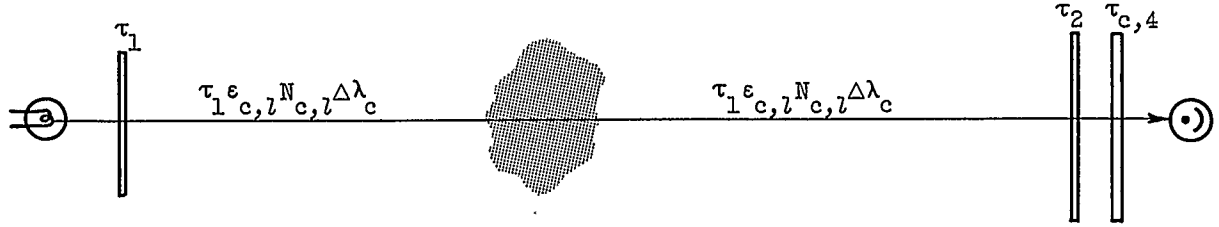

(b) Slit position, λ_c.

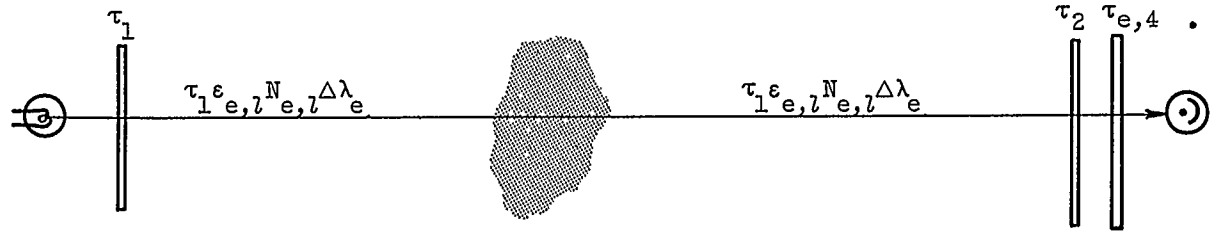

(c) Slit position, λ_e.

Figure 5. - Light-flux components for reversal equation for single-pass system.

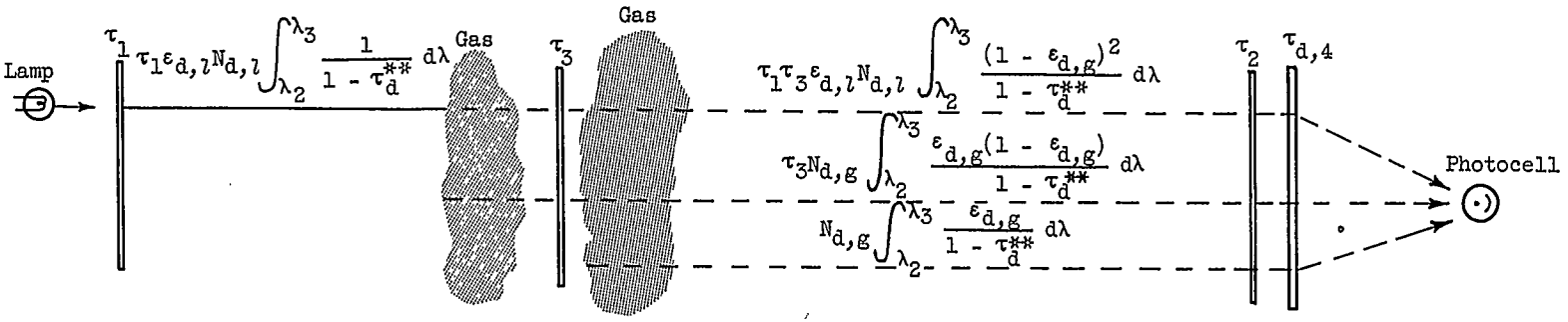

(a) Slit position, λ_d.

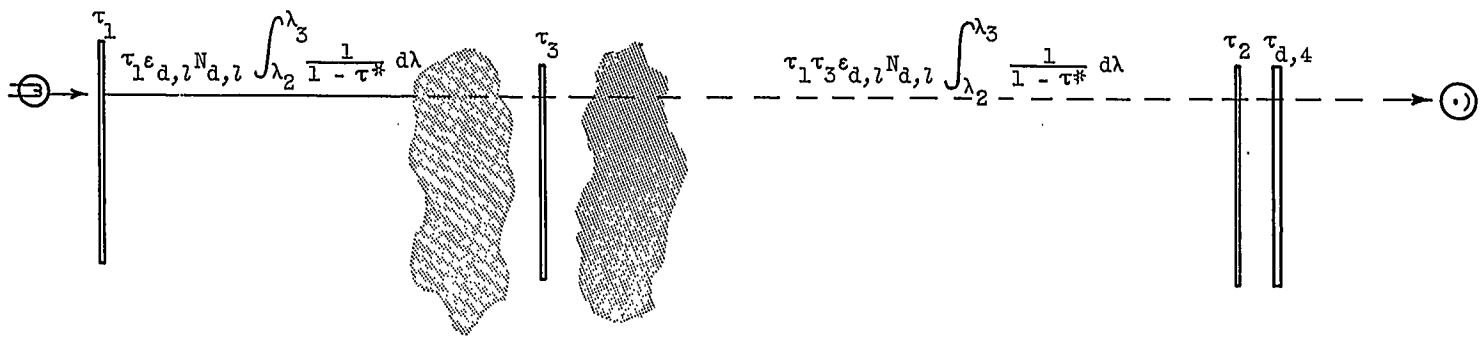

(b) Slit position, λ_h.

Figure 6. - Light-flux components for reversal equation with reflector for double-pass system.

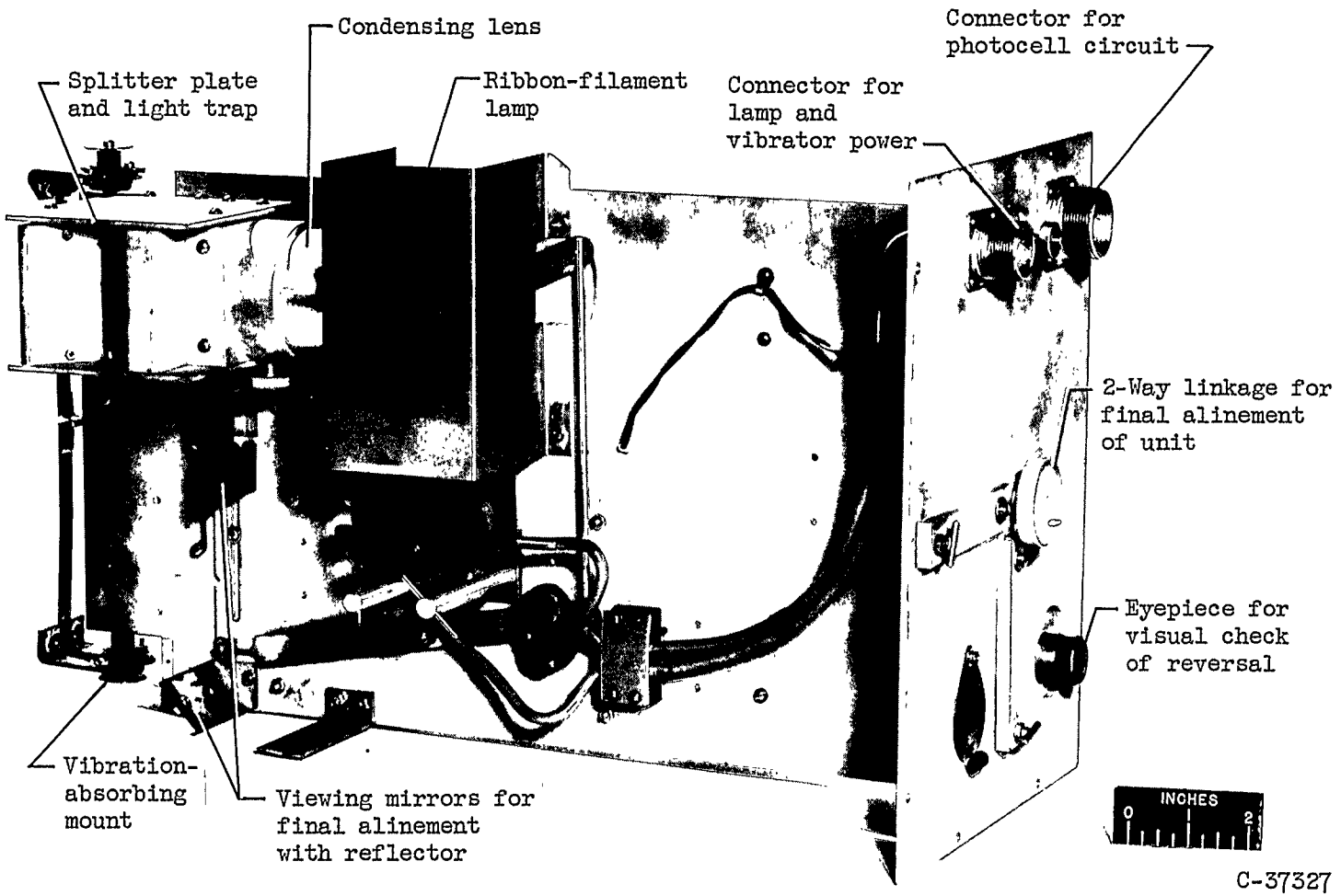

(a) Light-projection components.

Figure 7. - Optical unit.

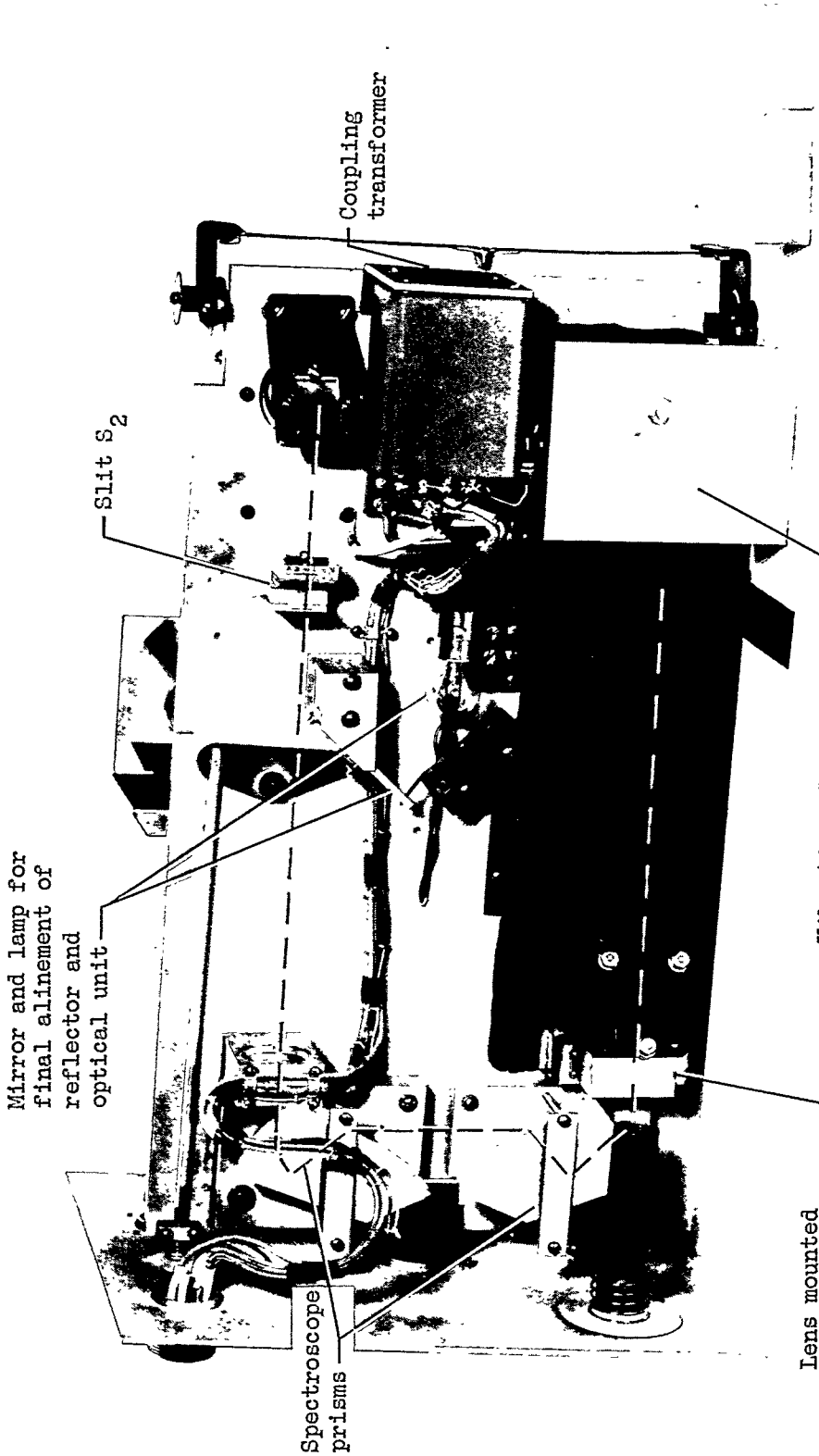

(b) Spectroscope and photocell components.

Figure 7. - Concluded. Optical unit.

CN-8 3797

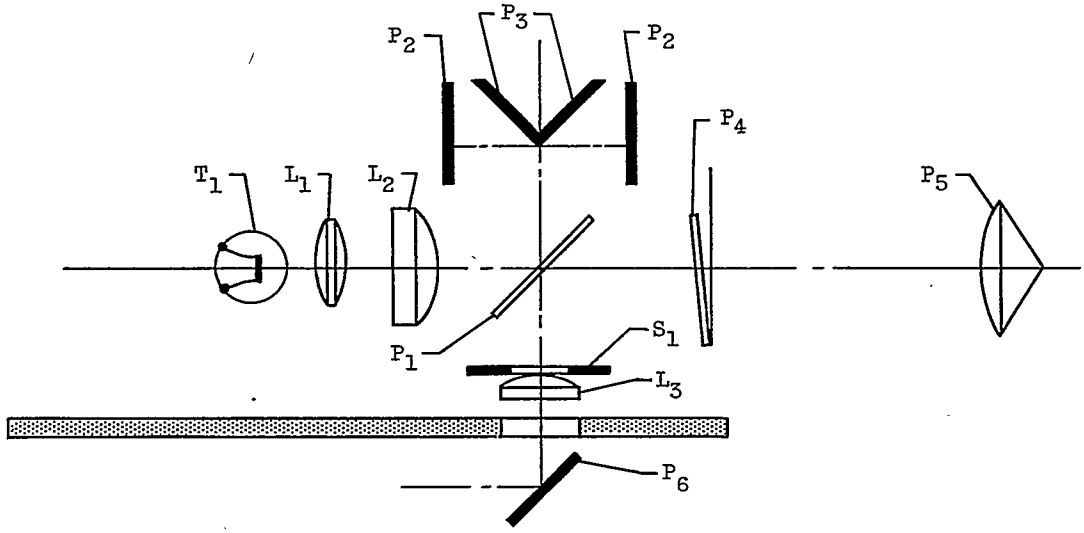

(a) Light source, top view.

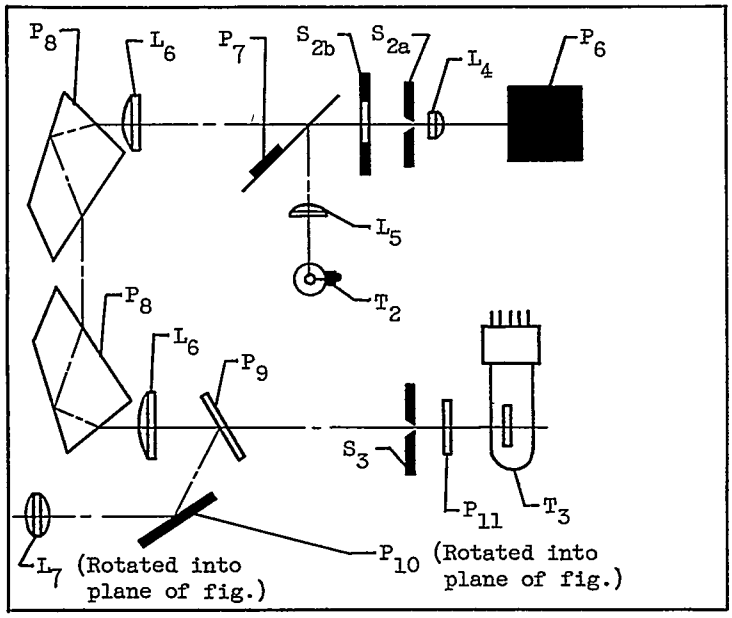

CD-4980

(b) Spectroscope, side view.

Figure 8. - Arrangement of optical components. (Symbols defined in table III.)

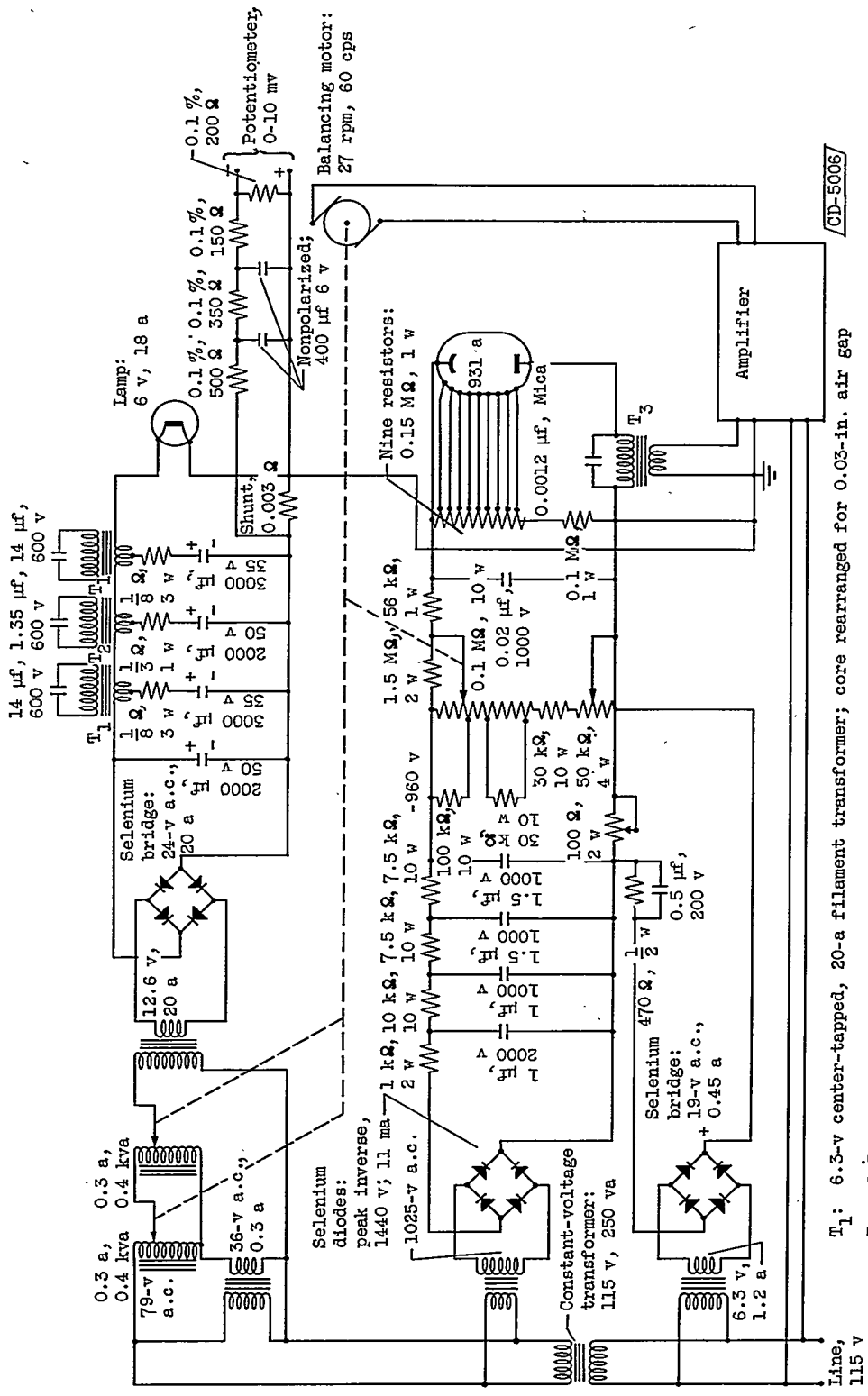

T_1: 6.3-v center-tapped, 20-a filament transformer; core rearranged for 0.03-in. air gap

T_2: 2.5-v center-tapped, 10-a filament transformer; core rearranged for 0.03-in. air gap

T_3: 80,000 to 50 Ω ; internal magnetic shield

T_1 and T_3 are tuned by the capacitors to resonance at 120 cps; T_2 is tuned by the capacitor to resonance at 240 cps

Figure 9. - Electric circuit.

CN-8 back 3797

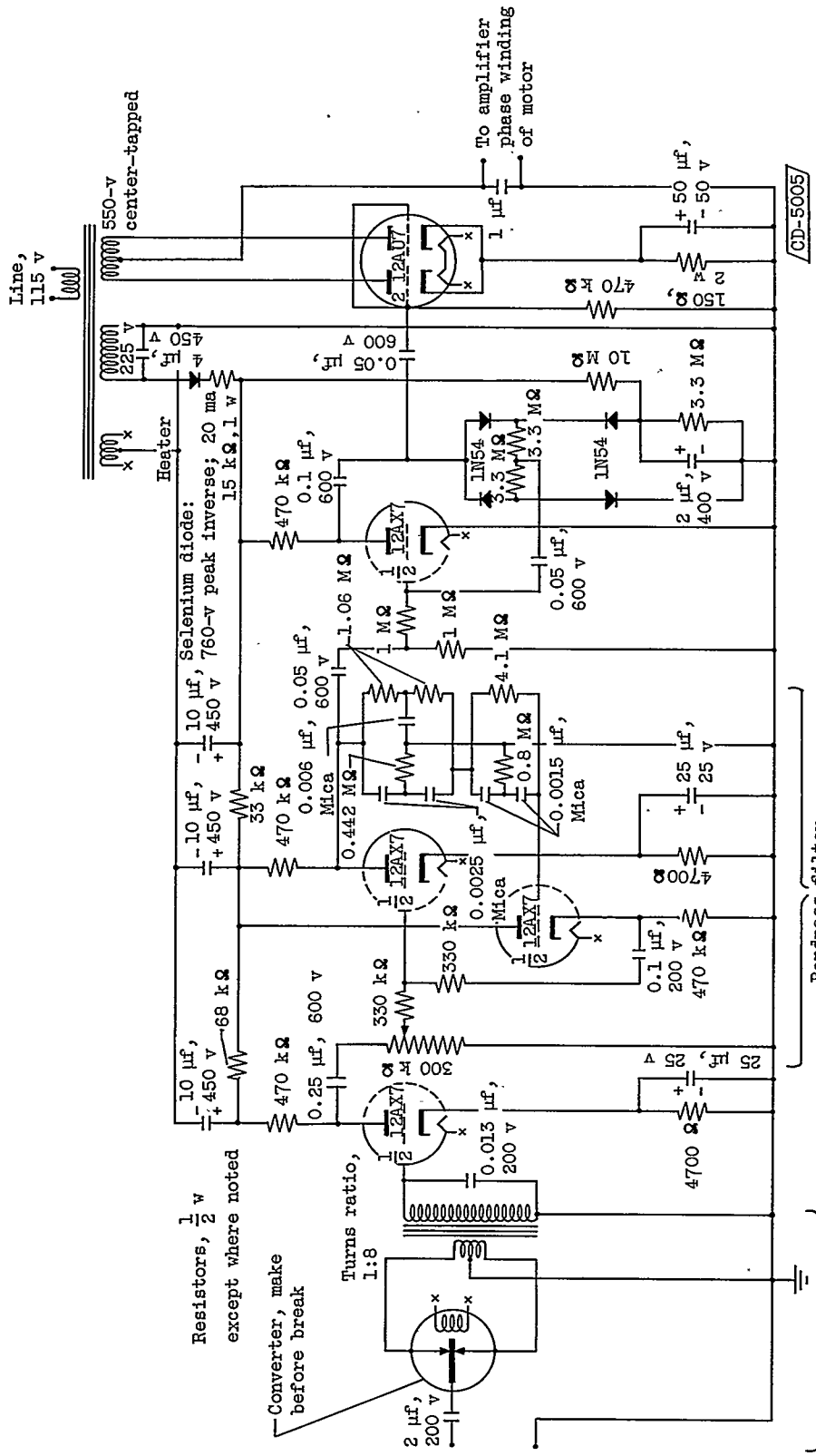

Figure 10. - Self-balancing amplifier circuit.

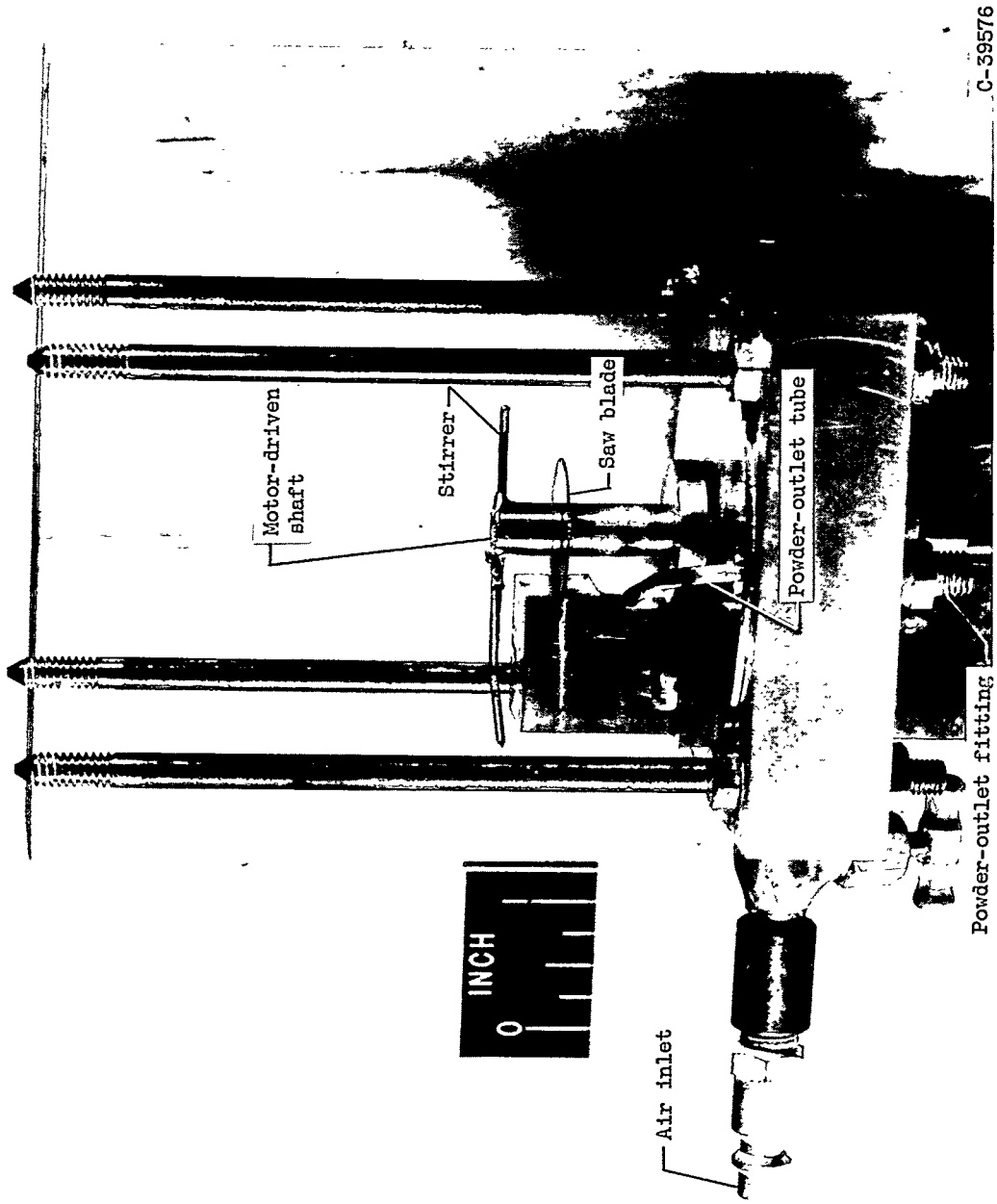

Figure 11. - Sodium-compound injector.

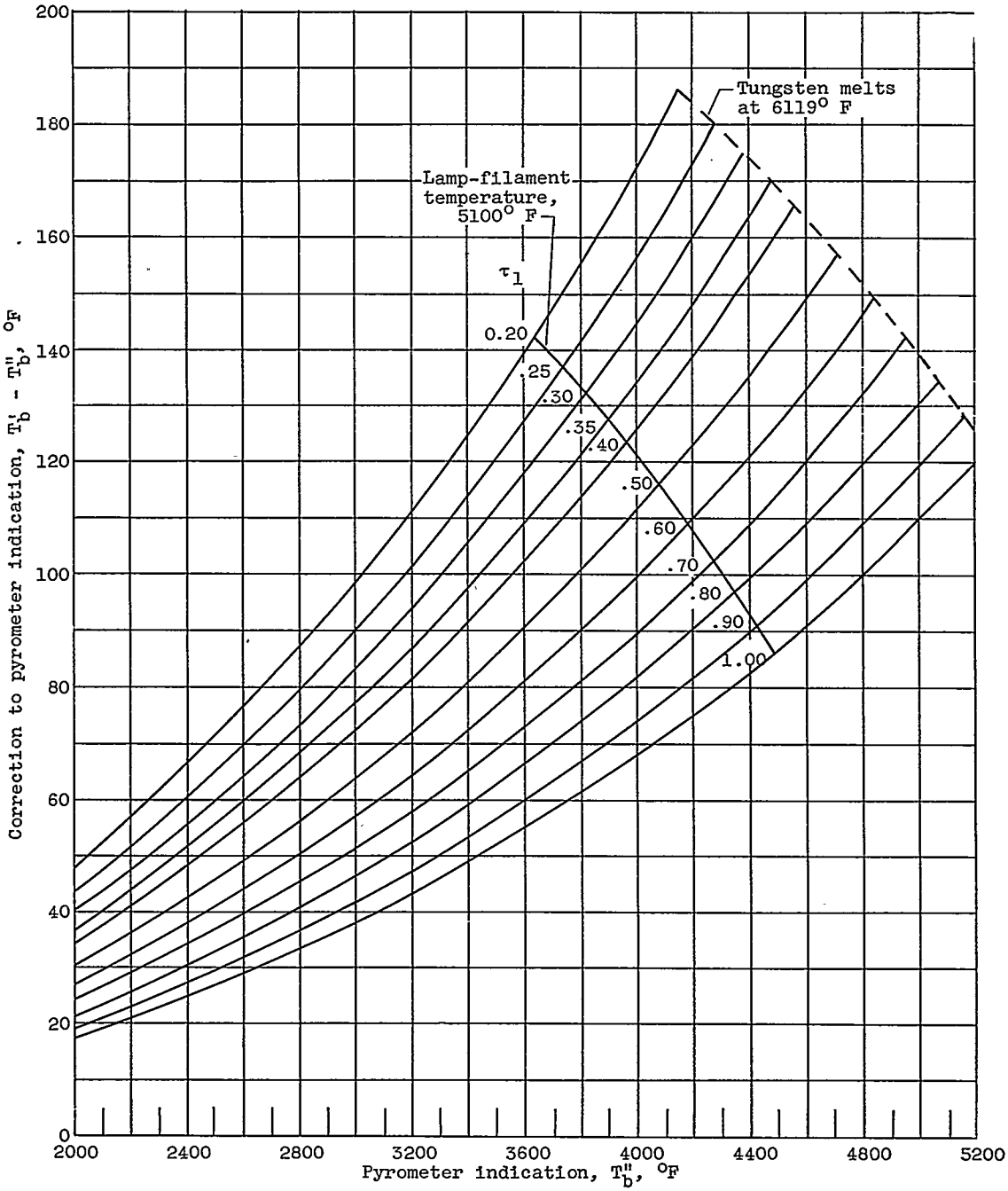

Figure 12. - Temperature correction for wavelength shift from 6650 A to 5893 A.

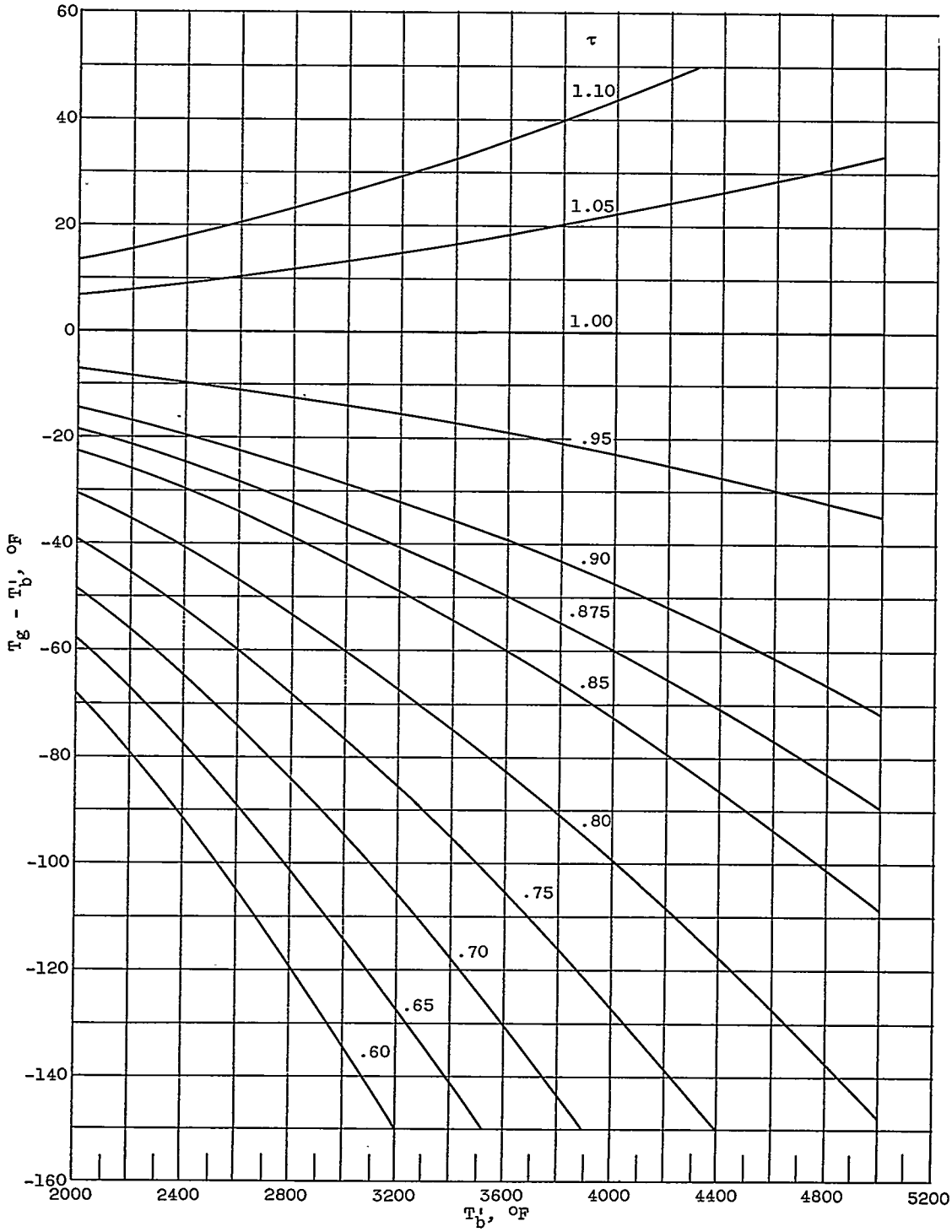

Figure 13. - Temperature correction for transmission factors at wavelength of 5893 A.

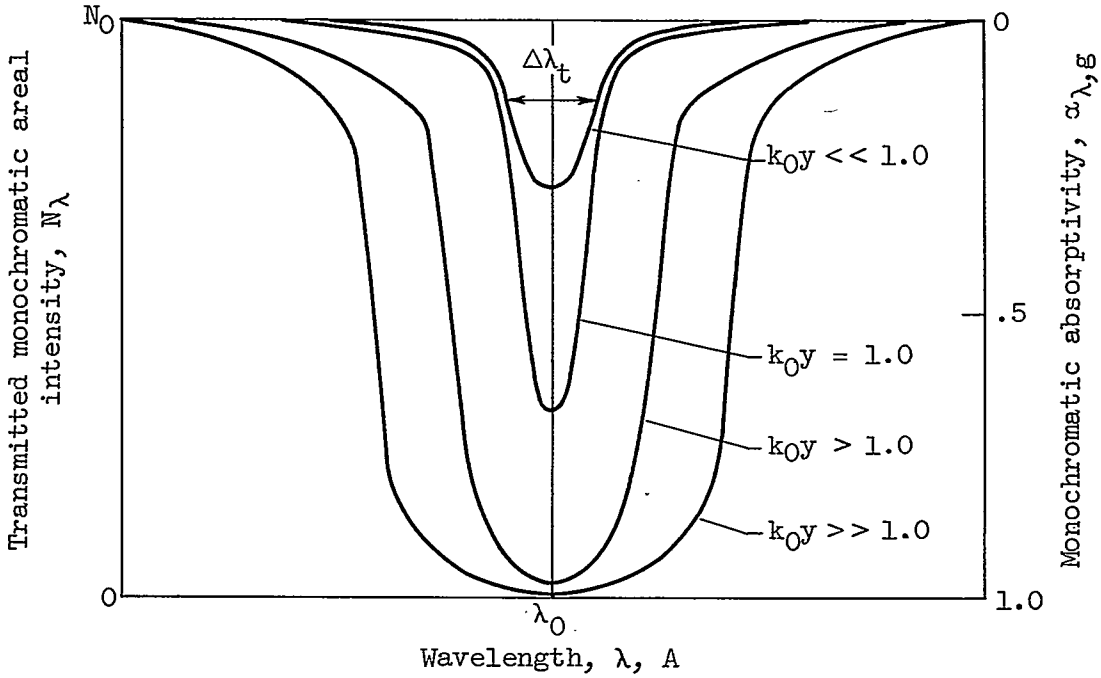

Figure 14. - Spectral absorption of one D-line at constant gas temperature.

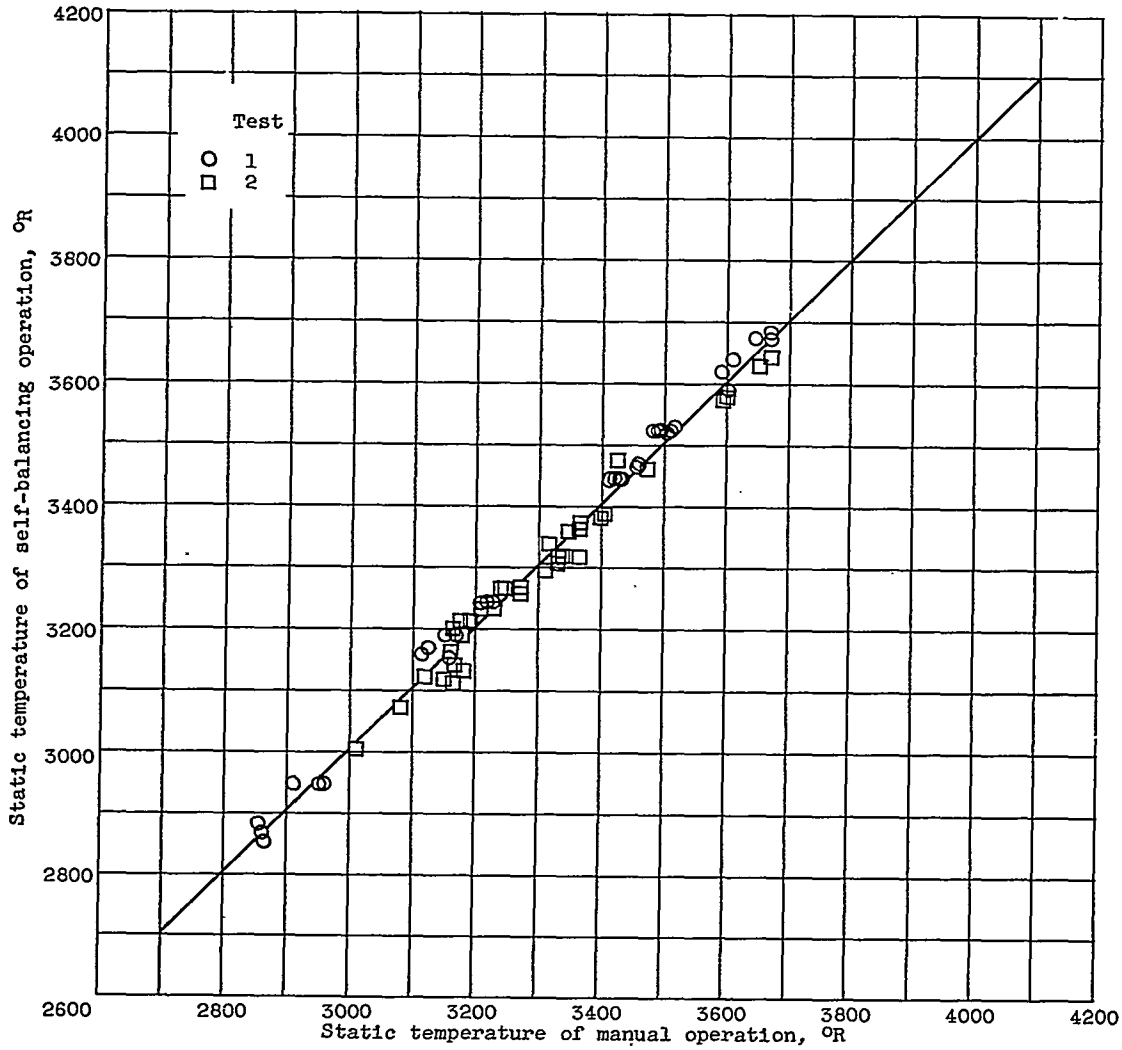

Figure 15. - Comparison of self-balancing and manual operations.

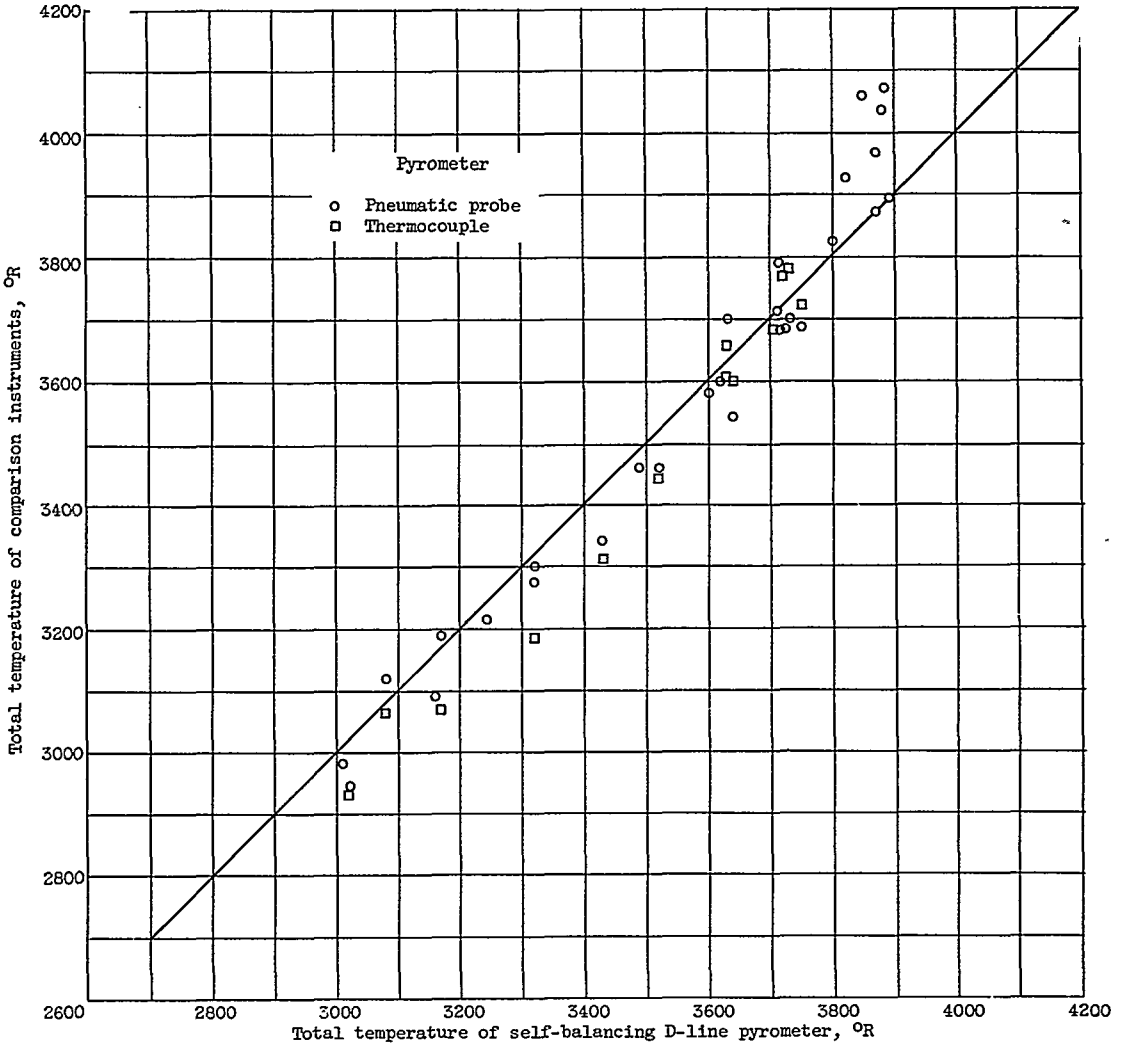

Figure 16. - Comparison of self-balancing D-line reversal pyrometer with pneumatic-probe and thermocouple pyrometers.

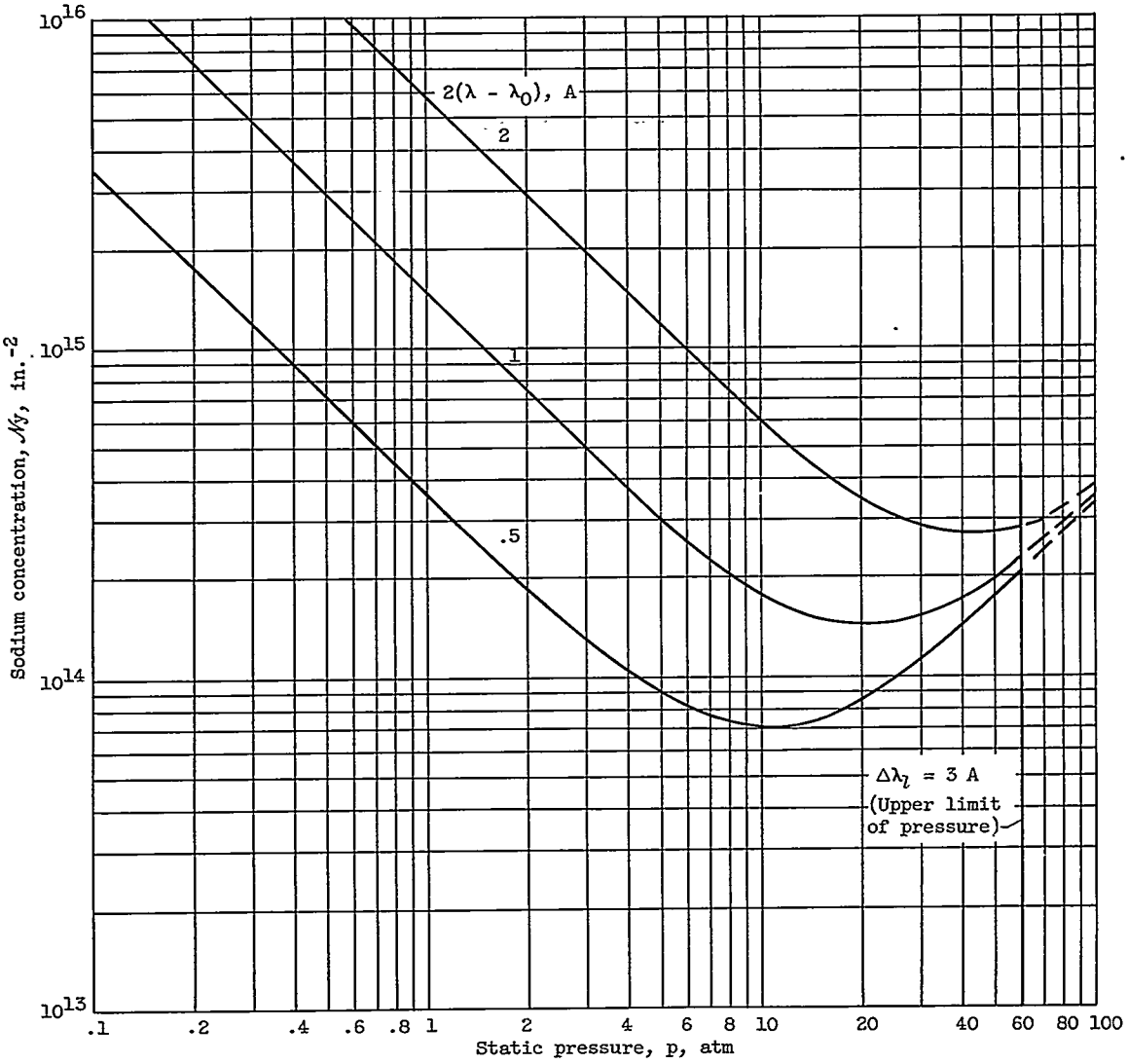

Figure 17. - Sodium concentration against static pressure. Temperature, 3700° R; wavelength, 5896 A; ε_λ, 0.5.

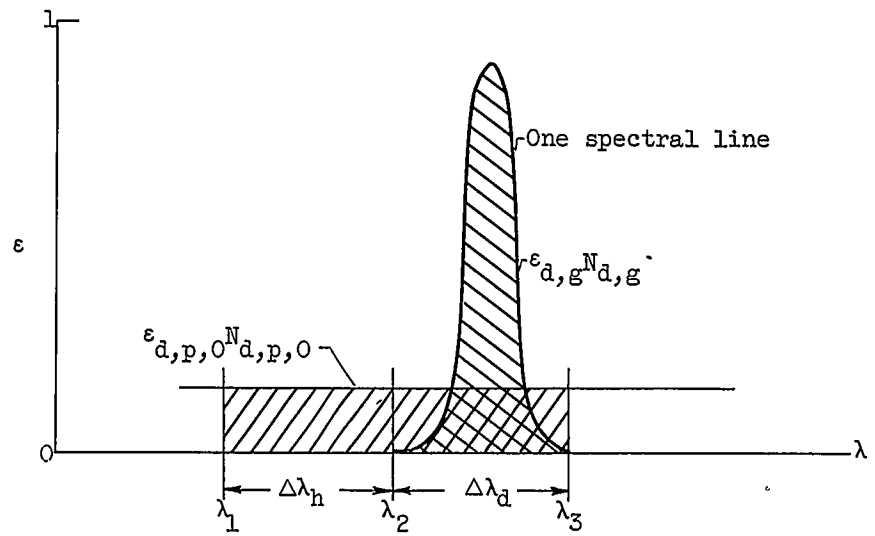

(a) Spectral emissivities.

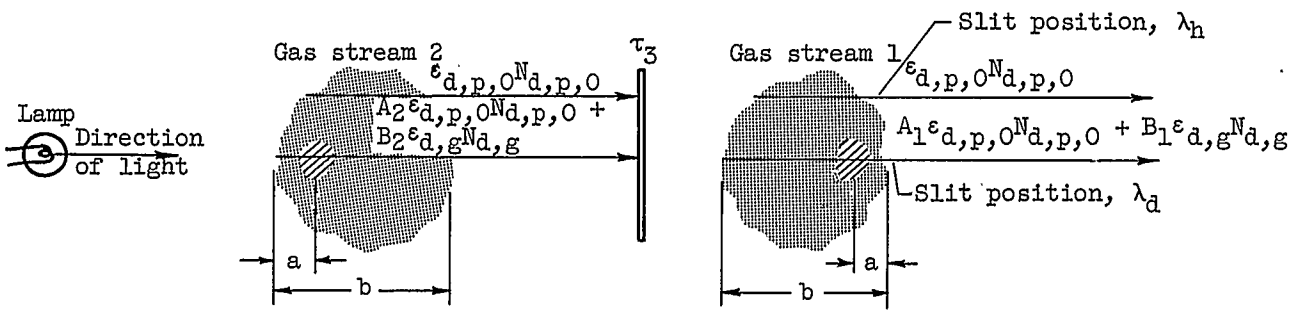

(b) Gas radiated intensity with sodium injected locally.

Figure 18. - Assumed model for luminous gas.

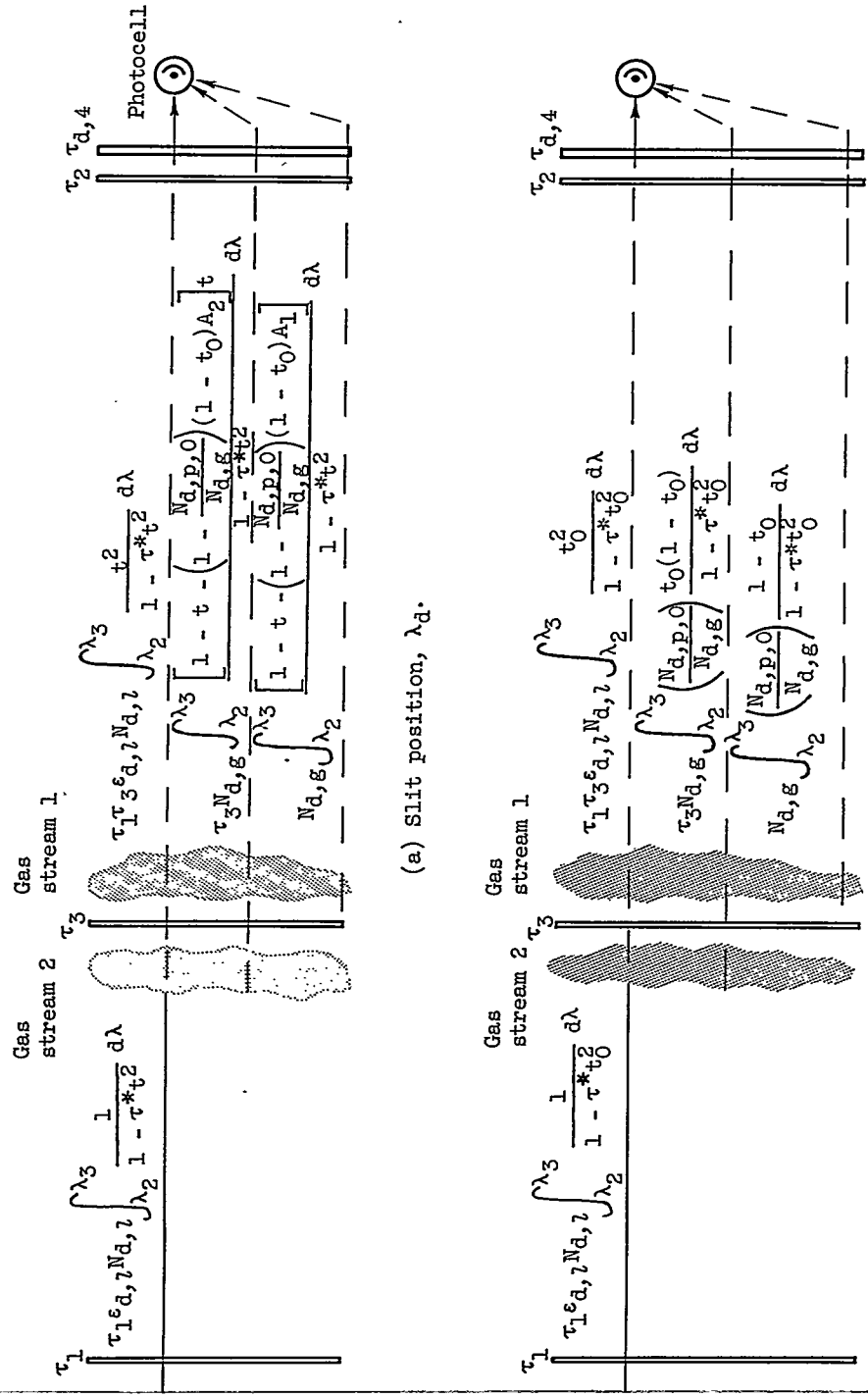

Figure 19. - Light-flux components for reversal equation with double-pass system and luminous gas.